EFFECTS OF POLAR STRATOSPHERIC CLOUDS IN THE NIMBUS 7 LIMS VERSION 6 DATASET

Ellis Remsberg[1] and V. Lynn Harvey[2]

[1]Science Directorate, NASA Langley Research Center
21 Langley Blvd, Mail Stop 401B
Hampton, Virginia 23681, USA

[2] Laboratory for Atmospheric and Space Physics
Atmospheric and Oceanic Sciences
University of Colorado, UCB 311
Boulder, Colorado, 80309, USA

Correspondence to: E. Remsberg (ellis.e.remsberg@nasa.gov)

Abstract. The historic Limb Infrared Monitor of the Stratosphere (LIMS) measurements of 1978-1979 from the Nimbus 7 satellite were re-processed with Version 6 (V6) algorithms and archived in 2002. The V6 dataset employs updated radiance registration methods, improved spectroscopic line parameters, and a common vertical resolution for all retrieved parameters. Retrieved profiles are spaced about every 1.6˚ of latitude along orbits and include the additional parameter of geopotential height. Profiles of O_3 are sensitive to perturbations from emissions of polar stratospheric clouds (PSCs). This work presents results of implementing a first-order screening for effects of PSCs using simple algorithms based on vertical gradients of the O_3 mixing ratio. Their occurrences are compared with the co-located, retrieved temperatures and related to the temperature thresholds needed for saturation of H_2O and/or HNO_3 vapor onto PSC particles. Observed daily locations where the major PSC screening criteria are satisfied are validated against PSCs observed with the Stratospheric Aerosol Monitor (SAM) II experiment also on Nimbus 7. Remnants of emissions from PSCs are characterized for O_3 and HNO_3 following the screening. PSCs may also impart a warm bias in the co-located LIMS temperatures, but by no more than 1-2 K at the altitudes of where effects of PSCs are a maximum in the ozone; thus, no PSC screening was applied to the V6 temperatures. Minimum temperatures vary between 187 K and 194 K and occur at or just above where the PSC effects are first identified in the ozone (most often between about 21 hPa to 28 hPa). Those temperature-pressure values are consistent with conditions for saturation and formation of supercooled ternary solution (STS) droplets and/or nitric acid trihydrate (NAT) aerosols. A temporary uptake of HNO_3 vapor by about 2-3 ppbv is indicated in mid-January downwind of and at pressure-altitudes where effects of PSCs are found. Seven-month, time series of the distributions of LIMS O_3 and HNO_3 are shown based on their gridded Level 3 data following the screening. The zonal coefficients of both O_3 and HNO_3 are essentially free of effects from PSCs on the 550 K surface as averaged at equivalent latitudes. Remnants of PSCs are still present in O_3 during mid-January on the 450 K surface. It is judged that the LIMS Level 3 data are of good quality for analyzing the larger-scale, stratospheric chemistry and transport processes during the Arctic winter of 1978-1979.

1 Introduction and Objectives

It is now well known that heterogeneous chemical reactions on surfaces of polar stratospheric clouds (PSCs) lead to an acceleration of the depletion of polar ozone in late winter and early spring (e.g., Solomon et al., 2015). Chemistry/climate models are showing that changes in the formation and persistence of PSC particles and of their related chemical effects are sensitive to changes in polar stratospheric temperatures, as well as to trends in ozone depleting substances (ODS). One current scientific need regarding stratospheric ozone is the "evaluation of the Antarctic ozone hole and Arctic winter/spring ozone depletion and the predicted changes in these phenomena, with a particular focus on temperatures in the polar stratosphere" (WMO, 2014). Therefore, it is important to characterize the occurrence frequency of PSCs, to compare their presence with the local temperature and chemical fields each winter/spring season, and to relate their current frequencies and effects with those of past decades.

The present study is an analysis for the effects of PSCs as determined for the Arctic winter of 1978-1979 from the Version 6 (V6) dataset of the Limb Infrared Monitor of the Stratosphere (LIMS) experiment on Nimbus 7 (Gille and Russell, 1984). This report of the LIMS PSCs supplements the Stratospheric Aerosol Monitor (SAM) II observations of McCormick et al. (1982) and provides a baseline prior to significant losses of Arctic ozone. It will be shown that emissions from PSCs lead to perturbations in the LIMS-retrieved ozone and that they occur at temperatures that are slightly colder than the saturation temperatures for nitric acid trihydrate (T_{NAT}). Those perturbations occur typically at altitudes that are 1 to 2 km below minimum temperatures (T_{min}) for the profiles. Criteria are described for the screening of the effects of the PSCs from the LIMS V6 species profiles. Daily surface maps are then generated from the screened dataset to compare the geographic location of PSC effects identified from LIMS to the PSCs observed by SAM II and to determine the extent to which there are residual effects in V6 ozone, nitric acid, and temperature. Time series of sightings of the effects of PSCs are shown and interpreted according to their associated temperature and potential vorticity distributions.

LIMS provided daily, along-orbit samplings of the effects of PSCs and of their co-located temperatures in the Arctic stratosphere, although it did not observe the winter season of the southern hemisphere. An early analysis of the LIMS Version 5 (V5) Level 2 (or profile) dataset was conducted for evidence of emissions from PSCs, and those initial results were reported at a NASA Workshop (Hamill and McMaster, 1984). Figure 1 reproduces a V5 ozone mixing ratio profile of 11 January from the Workshop report, and it shows a large, spurious excess of ozone centered near 50 hPa that was attributed to effects of emissions from PSCs. The LIMS radiance profiles were re-processed in 2002 using Version 6 (V6) algorithms to obtain profiles of temperature, chemical species, and an additional quantity, geopotential height, as a function of pressure-altitude from about 65˚S to 84˚N latitude (Remsberg et al., 2004).

Spang et al. (2016) give a very good survey of the occurrences of PSCs in the Arctic (and Antarctic) winter stratosphere and over many winters. They provide excellent inferences about the likely PSC composition based on the spectral features in their satellite limb radiances and on the polarization characteristics of the PSC particles gained with co-located satellite lidar return signals. Spang et al. (2016) also provide information on the co-located environmental temperatures. The LIMS V6 data yield complementary findings about the occurrences of PSCs from their effects in the retrieved V6 ozone profiles plus co-located V6 temperature distributions from the same satellite sensor, but for the much earlier period of 1978-1979. Estimates of the uptake of HNO_3 vapor are given herein for that early period for the first time. Finally, we report that there is almost no interference from PSCs in the distributions of the Level 3 HNO_3, such that one can analyze for the relative contributions of chemistry versus transport in their time series throughout the lower stratosphere.

The findings from LIMS V6 are organized as follows. Section 2 contains background information on the LIMS experiment, its earlier V5 dataset, and improvements from V6. Section 3 includes a characterization of the mapped distributions of ozone, nitric acid, temperature, and geopotential height from V6. It is shown that there is a good relationship at 31.6 hPa between the highest values of nitric acid vapor, lowest values of ozone, and lowest values of geopotential

height (polar vortex region). Section 3 then describes criteria for screening the effects of significant emissions from PSCs using the V6 ozone and compares them to the effects in HNO_3 and temperature. Section 4 explains that there can be "false positives" of effects from PSCs but that those instances are rare until early February 1979. Section 5 is a summary of the occurrences of Arctic PSCs and their associated temperatures for the winter of 1978-1979; the daily instances are archived in separate files.

Section 6 compares the findings for temperature, HNO_3, and O_3 with estimates of the composition and temperature thresholds from more recent measurements of PSCs and from microphysical models for the formation of PSCs. It is shown that significant zonal wave-1 forcings bring about rapid exchanges of O_3 and HNO_3 between middle and polar latitudes in early December and late January (e.g., Leovy et al., 1985). The mapped data and the time series analyses are examined for instances of uptake or loss of HNO_3 vapor as well as instances of the advection of low values of O_3 and HNO_3 to the vortex from lower latitudes. Section 7 provides evidence for a temporary uptake of HNO_3 vapor onto PSC particles, when the temperature is less than 194 K. The findings of uptake from LIMS V6 are also compared with independent determinations in the literature. Section 8 then shows the evolution of O_3 and HNO_3 with respect to potential vorticity for the entire 7+ months of the LIMS experiment. Those time series are based on the LIMS Level 3, zonal Fourier coefficients derived from the profile data, and it will be shown that they are essentially free of PSC effects on the 550 K potential temperature surface (near 31.6 hPa) but that there are some remaining perturbations in the ozone of mid-January on the 450 K surface (near 46.4 hPa). Both species show the combined effects of meridional transport and mixing during the winter months. Section 9 summarizes the primary findings of this study.

2 Overview of the effects of clouds in the LIMS measurements

This section reviews findings about cirrus clouds and PSCs from LIMS V5 and the changes adopted for their sensing with V6. LIMS obtained profiles of atmospheric limb radiance in six instrument channels, a wide and a narrower band channel for CO_2 (CO_2W and CO_2N) and one

each for O_3, H_2O, HNO_3, and NO_2. The bandpass filters (in cm^{-1}) for the channels are CO_2W (579-755), CO_2N (637-673), O_3 (926-1141), H_2O (1370-1560), HNO_3 (844-917), and NO_2 (1560-1630) in terms of their 5% relative response points. Temperature is retrieved based on the CO_2W channel radiances below about the 10-hPa level. The channels for H_2O and NO_2 have an instantaneous field-of-view (IFOV) vertical width of 3.6 km at the horizon, while the other four channels have half that width or 1.8 km (see Gille and Russell (1984) and Remsberg et al. (1990) for more details about the LIMS instrument and the domain of its atmospheric measurements).

Radiances in the LIMS species channels are affected by emissions from cloud tops, and the retrieved LIMS mixing ratio profiles contain features due to them. None of the LIMS species channels have a bandwidth that is free of their target gases, such that one can attempt to characterize emissions from only the clouds and/or aerosols. For the sensing of PSCs from their radiances about the best that one can do is to consider anomalies in profiles of the ratio of the water vapor radiance to the CO_2W radiance. But the IFOVs of the H_2O and CO_2W channels are not compatible, which means that one cannot properly account for the corresponding radiances from temperature itself. Effects of emissions from clouds are delineated best with the narrow-IFOV, O_3 and HNO_3 channels. Yet, cloud occurrences are more pronounced in the retrieved O_3 than in HNO_3 because the relation between mixing ratio and radiance is non-linear for LIMS O_3. Pressure-altitude locations of perturbations from cloud tops are included in a header line for every V6 profile, so that effects of the clouds can be screened from them prior to their processing with the LIMS Level 3 mapping algorithm (e.g., Remsberg et al., 1990).

Although the spectral effects of emissions from PSCs were not understood well in the 1970s, there are obvious effects from them in the LIMS retrieved ozone (Fig. 1) and in H_2O (not shown). Since the ozone channel has a vertical IFOV width that is half that of the H_2O channel, it is easier to obtain an accurate vertical location of the effects of PSCs from the retrieved ozone. The archived profiles carry a pressure-altitude or p(z) index of where the perturbing effects of PSCs are first noted in the ozone profiles. However, profile segments that are affected by those emissions were not screened out prior to their insertion into the V5 mapping algorithm; instead,

their presence showed up clearly as “bull’s-eye-like” features or as localized ozone maxima in preliminary maps of the daily parameters on pressure surfaces. Those occurrences are reported in Remsberg et al. (1986, their Tables 6 and 7 and Fig. 4). Then, the vertical segments that gave rise to them were removed using conservative latitude/longitude templates of the affected regions followed by a final mapping of the V5 profile data.

The same PSC templates were applied in the map analyses of the V5 temperatures, and the maps were inspected for evidence of perturbing effects (Remsberg et al., 1986, their Appendix A). Independently, Austin et al. (1986) compared the V5 temperature profiles with those from the TIROS-N Stratospheric Sounding Unit (SSU) for the winter Arctic vortex region, and they found that the SSU T was colder at 30 hPa on average than that of V5, but not by much (SSU minus LIMS T = -0.8 ± 2.8 K). They noted that the pressure modulation radiometry (PMR) measurement technique of the SSU sensor is essentially unaffected by interfering emissions from PSCs. Thus, Austin et al. (1986) concluded that the V5 temperature profiles were perturbed very little at 30 hPa by radiances from the PSCs.

Austin et al. (1986) and Remsberg et al. (1986) reported that the locations of effects of PSCs in the V5 data agreed well with independent determinations of PSC extinction from the SAM II experiment, when their measurements overlapped spatially. Further, McCormick et al. (1982) reported moderate levels of extinction from SAM II PSCs at altitudes between 17 and 20 km and with co-located temperatures of 193 and 196 K, according to gridded analyses provided to them by the NOAA Climate Prediction Center (CPC). They also reported that minimum temperatures from the CPC analyses ranged from 192 to 194 K and occurred at altitudes of 19 to 22 km or several kilometers above where PSC extinctions were maximum. Based on the foregoing realizations, it is likely that T_{min} from the LIMS profiles is within its estimated uncertainties and can be used to define the atmospheric environment for PSC formation. Therefore, it was decided that no screening for PSC effects would be applied in the algorithm for the temperature profiles of V6. This approach means that the V6 temperature and associated geopotential height profiles are spaced continuously along the orbits and extend down to the cloud tops or near to and below

192 the tropopause, which is helpful for their assimilation into atmospheric models for studies of
193 stratospheric transport.

194

195 Improvements that were implemented for V6 include a better registration for the LIMS
196 radiances and the use of updated spectroscopic line parameters for retrievals of the species
197 profiles. In addition, the retrievals for V6 were conducted for each profile pair at a spacing of
198 1.6˚ of latitude (at the Equator) along orbits, instead of every 4˚ as with V5. A screening for the
199 effects of the PSC emissions was conducted for the V6 species profiles. Remnants of PSC
200 effects are present in ozone and water vapor (H_2O), but are much less apparent in nitric acid
201 (HNO_3) vapor and nitrogen dioxide (NO_2). Thus, one can effectively look for any changes in
202 HNO_3 and NO_2 adjacent to the PSCs because their fields have little contamination. Emissions
203 from PSCs are minimal in the LIMS 15-μm CO_2 radiances, and their effects are nearly absent in
204 the V6 temperatures. More importantly, the V6 temperature and species profiles have a
205 common effective vertical resolution of 3.7 km, yielding co-located profile parameters that are
206 compatible spatially. As a result, the LIMS V6 dataset is judged of good quality and is part of
207 the SPARC Data Initiative (e.g., Tegtmeier, et al., 2013).

208

209 Retrievals of the V6 temperature and associated species were obtained by using all successive,
210 up/down scan profile pairs along their observed, orbital tangent-path locations and at p(z) levels
211 spaced about every 0.88 km. Thus, spurious perturbations in the retrieved ozone are recorded
212 with better vertical and along-orbit sampling than was the case for the V5 data analyzed by
213 Austin et al. (1986). A screening was performed and V6 species profile segments removed, as
214 follows. First, entire profiles were deleted whenever the ozone mixing ratio was greater than 20
215 ppmv within the pressure-altitude range of 0.2 to 50 hPa. Those rare instances are attributed to
216 perturbations in the motion of the instrument scan mirror that affected the subsequent registration
217 of the associated, measured radiance profiles. Then, a further screening for emissions from
218 cirrus clouds was conducted based on instances of abrupt increases in ozone mixing ratios in the
219 region of the tropopause. That screening was conducted below the 45-hPa level equatorward of

30˚ latitude and below the 100-hPa level poleward of that, as discussed in Remsberg et al. (2007).

3 Detection and screening of effects of PSCs for LIMS V6

a. Meteorological context

This section considers effects of PSCs in the V6 retrieved species and temperatures, presents the geographical evolution of remnants of PSCs following their first-order screening, and compares the location of those remnants with extinction observations from SAM II. As an example, Figure 2 shows northern hemisphere polar plots of the V6 Level 3 ozone, geopotential height, temperature, and nitric acid vapor at 31.6 hPa for 11 January, a day when ozone profiles in the region of the polar vortex are contaminated by PSCs. The Level 3 algorithm consists of zonal Fourier coefficients for the mean and wavenumbers 1-6 that are obtained with a sequential estimation technique and are available at every 2˚ of latitude and on pressure surfaces having a vertical spacing of about 2.7 km (Remsberg and Lingenfelser, 2010). The V6 mapping algorithm was applied separately to sequences of profiles along each latitude circle. Since only a few profiles were perturbed and screened from the input files for each day, the mapped ozone of Fig. 2 displays the medium and large-scale variations accurately based on a gridding of those daily zonal coefficients at a longitude resolution of 5.625˚. The good continuity of the ozone fields with latitude in Fig. 2 is a separate measure of the precision of the orbital data. At this point it is stressed that the species profile segments that were screened of significant effects from PSCs are not part of the input ozone data for Fig. 2. Thus, the centroid of ozone at about 70˚N, 270˚E that exceeds 4 ppmv is the result of the mapping of residual effects of emissions from the PSCs that are still present in the Level 2 profiles. Locations of ozone profile segments for 11 January that were flagged and screened out are indicated by the white plus signs in the panels of Fig. 2. Thus, it is the neighbors of those flagged ozone profiles (and not the flagged profiles themselves) that contribute to the excess ozone features in Fig. 2.

McCormick et al. (1982, their Table 1 and Figure 3) reported a moderate level of stratospheric aerosol extinction at 1.0 μm wavelength and centered at 18 km on 11 January 1979. The solid red dot in Fig. 2 is the location of that SAM II observation or just north and west of Hudson Bay, Canada, at 67˚N, 257˚E; it is at the edge of the excess of V6 ozone, indicating that PSC extinctions to the north were likely larger that day than what SAM II observed. It is also noted that the region of elevated ozone is where the LIMS temperatures are coldest (<196 K) and near the center of the polar vortex, as defined by the LIMS geopotential height field.

b. Screening criteria for PSCs in ozone

The LIMS V6 Level 2 screening criteria are described as follows. The primary criterion is denoted by a parameter labeled DIF in the daily files of ozone data points that were screened out. The DIF threshold was evaluated and then finally set as an absolute mixing ratio change of greater than 1.7 ppmv between two adjacent LIMS ozone profile points, spaced 0.88 km apart. As an example, Figure 3 shows five successive V6 ozone profiles from 11 January along the orbital tangent path from 63.2˚N to 68.4˚N and 258.2˚E to 260.6˚E. All five ozone profiles have similar values in the upper stratosphere, but their apparent mixing ratios differ markedly between 40 and 50 hPa. The V6 profile at 68.4˚N is equivalent to the V5 ozone of Fig. 1, and the DIF criterion for the V6 profile was met at the 31.6-hPa level. The level designated as free of PSC effects was set at four points above that, as denoted by the horizontal line at 19 hPa in Fig. 3 in order to account for the finite FOV effects of the LIMS measurement and the vertical resolution of 3.7 km for its retrieved ozone. That profile and several adjacent ones poleward along the orbit were screened of effects from PSCs, as noted by the white plus symbols in Fig. 2. The DIF value is 2.2 ppmv for the V6 profile equivalent to that in Fig. 1, and it occurs at 31.6 hPa.

A secondary criterion is based on the absolute value of the ratio *f* (labeled as an RTO parameter in those same data files) and defined as

$$f = [q(n) - q(n-1)] / q(n-1) \quad . \qquad (1)$$

Specifically, the RTO threshold was met when there was a change in the ozone mixing ratio *q* with decreasing altitude between two adjacent profile points, *n-1* and *n*, (spaced 0.88 km apart) such that *f* in Eq. (1) was greater than 0.7 whenever *q(n-1)* had a somewhat arbitrary value of greater than 0.5 ppmv. Note that the point index *n* for a profile in the data file increases as altitude decreases, due to the nature of the "top-down" retrieval algorithm. As with DIF, the screening based on the RTO criterion begins four points above where the threshold is met. The RTO threshold is complementary to DIF and accounts for occurrences of anomalous vertical structure in ozone, where the ozone mixing ratio is small (but > 0.5 ppmv). Only two profiles met the RTO threshold on 11 January (near 82˚N, 180˚E), and they occurred at the level of 88 hPa. The DIF threshold was also met for one of them at that level.

Another situation is shown by the long dashed profile for 67.1˚N, 259˚E in Fig. 3, where the ozone between 27.8 and 31.6 hPa reaches an upper limit, DIF value of 1.6 ppmv while the RTO value is only 0.23; the DIF and especially the RTO values are under the thresholds for perturbing effects from PSCs such that this profile survives the somewhat liberal screening criteria. Ozone profiles in Fig. 3 just equatorward of the PSC-screened profile are included in the surface maps of O_3 and HNO_3 shown in Fig. 2, even though they also contain residual effects of emissions from PSCs. The zonal mapping algorithm for a given latitude responds to the residual features of 11 January and also to any perturbations that may have occurred on the several days both prior to and following it. One final screening criterion was imposed based on whenever the retrieved ozone mixing ratio dropped below 0.2 ppmv. Such small values were assigned to the tangent layer as a consequence of a matching of the calculated forward radiances to the measured radiances, which is inherent in the onion-peeling retrieval method of LIMS. Those rare occurrences are considered a "false positives" for PSCs, and they are discussed in Section 4.

c. Temperature profiles

Knudsen (1996) determined that PSCs composed of water ice do not form until the environmental temperatures become low enough to achieve saturation, T_{ICE}, of 186.4 K at 30 hPa (≈22.6 km) or of 189.2 K at 50 hPa (≈18.6 km), based on a nominal water vapor mixing ratio of

5 ppmv. However, he also noted that those conditions are not met most times; coldest temperatures in the vicinity of PSCs are often a few degrees warmer than T_{ICE} (see also McCormick et al., 1982; Hamill and McMaster, 1984; Austin et al., 1986). Later, Crutzen and Arnold (1986) and Schlager and Arnold (1990) reported that the occurrence of PSC particles is more consistent with saturation conditions for nitric acid tri-hydrate (NAT). Knudsen (1996) calculated threshold temperatures for the formation of NAT (T_{NAT}) of 192.9 K at 30 hPa and of 195.5 K at 50 hPa, based on water vapor of 5 ppmv and a January LIMS nitric acid profile at 76˚N, having values of the order of 10 ppbv at 30 hPa and 7 ppbv at 50 hPa. In addition, the retrieved temperatures remain cold (~196 K) from 53 to 88 hPa for the two cases where the LIMS RTO threshold is met at 88 hPa, and they are even colder (~193 K) at 150 hPa or 13 km.

Figure 3 also shows two co-located LIMS V6 temperature profiles for 64.5˚N and 68.4˚N, and they have minima of 193.9 K at 24.5 hPa and 191.9 K at 16.7 hPa, respectively, or near to T_{NAT}. Temperatures at 46 hPa are warmer by 3 K and 6 K, respectively, or where the associated, perturbed ozone mixing ratios are largest. Note that the temperature profile at 64.5˚N has its minimum at 24.5 hPa and then rises smoothly toward higher pressures, while the temperature profile at 68.4˚N is slightly warmer than the one at 64.5˚N from about 35 to 60 hPa. This finding indicates that the retrieved temperatures at 68.4˚N are perturbed slightly by emissions from PSCs at pressures levels where their perturbing effects on ozone are largest.

Figure 4 shows the effects of the perturbations at 46 hPa more clearly. Locations of the PSC contaminated profiles of 11 January in Fig. 2 are not over plotted on Fig. 4, although the SAM II sighting has been retained. The ozone panel of Fig. 4 shows maximum ozone remnants due to PSCs at about 75˚N, 270˚E. The corresponding panel for temperature shows values in the same location that are lighter blue or a bit warmer (>196 K) compared with colder values (<196 K or darker blue) at adjacent longitudes, even though both locations are within the polar vortex (see panel for geopotential height). That region of slightly elevated temperatures is very likely the result of not screening for effects of PSCs from the V6 temperature profiles.

At this point it should be clear that there are significant residual effects of PSCs in ozone at 31.6 hPa (Fig. 2), but that they are essentially absent in the temperature. Thus, it is possible to know where PSCs are located based on the ozone field, but also to be confident that there is little impact on the co-located temperature fields and no impact on the geopotential height fields for calculations of the associated species transport. It is presumed that the LIMS temperatures are within their estimated accuracies at and above where the effects of PSCs are small in the co-located ozone. Tighter criteria can screen out more instances of PSC contamination from the species but may also remove some profile segments having vertical structures due to real, transport-induced effects. In particular, a few instances of an overly tight screening have been found based on the RTO criterion at pressure-altitudes from 52.7 to 100 hPa, as indicated by co-located temperatures that are much too warm for saturation and maintenance of PSC particles.

d. Nitric acid

The LIMS-retrieved O_3 and H_2O have non-linear sensitivities to radiance or temperature biases (Remsberg et al., 2004). Distributions of LIMS NO_2 are affected too, primarily because of the need to correct its radiances for interfering effects from the perturbed H_2O. However, HNO_3 is affected much less as shown in its corresponding panel of Fig. 2 because the relationship between the observed HNO_3 radiance and retrieved mixing ratio is nearly linear. In support of that finding, simulation studies show that a temperature bias error of 1 K has only a small, 3% effect on the retrieval of HNO_3 between 10 to 50 hPa (Remsberg et al., 2010, their Table 1). In addition, there are no clear anti-correlations between the distributions of temperature and nitric acid in Fig. 2; for example, relatively high values of HNO_3 are found in both the cold vortex region near the Pole and toward the much warmer Aleutian sector. This finding of a small anti-correlation between temperature and HNO_3 is a consequence of the weak chemical reactivity of vapor phase HNO_3 in the polar night (Brasseur and Solomon, 2005).

To what degree are there PSC remnants in the V6 HNO_3? As examples, it was shown in Figures 2 and 4 that there are remnants of PSCs from 260-360˚E in ozone at 31.6 hPa and 46.4 hPa on 11 January and perhaps a slight excess in the nitric acid field in the same region. Figure 5 shows the

V6 HNO_3 profiles for 11 January that are co-located with the screened ozone profile and adjacent ones of Fig. 3. Note that the maximum value of nitric acid for the unscreened HNO_3 profile in Fig. 5 is about 13 ppbv from 30 to 50 hPa or essentially not much different from that at about 75˚N, 140˚E in Fig. 2, where no effects of PSCs are indicated. It is also apparent from Fig. 2 that the HNO_3 vapor is only 10 ppbv in a small region near 80˚N, 0˚E and "downwind" of the PSCs over northern Greenland. The corresponding temperature profile at 67.1˚N, 258.9˚E in Fig. 5 has a minimum value of 192.1 K, which is cold enough for condensation of HNO_3 vapor onto droplets of STS.

McCormick et al. (1982) also found PSCs from 18 to 22 January 1979, and they reported co-located temperatures that were very cold. SAM II PSC extinction values for 18, 19, and 22 January 1979 are an order of magnitude greater than on 11 January. Accordingly, Figure 5 also shows a LIMS nitric acid profile for 19 January adjacent to one that was screened out along the same orbit and located very near to the profile of excessive PSC extinction found by SAM II at 67.8˚N, 43˚E. The V6 HNO_3 profile has a maximum value of 17 ppbv at about 25 hPa or an excess of perhaps 4 ppbv compared with the more nominal profile of 11 January. Thus, the HNO_3 response to those much larger PSC extinction values is definitely elevated, but not to the same extent as the ozone response. The co-located LIMS temperature profile for 19 January is also shown in Fig. 5, and it has a minimum value of 190.1 K at 25 hPa.

4 Anomalous indications of effects of PSCs from V6

SAM II observed maximum extinctions from PSCs at about 68˚N, 30˚E and near 22 km on 18 and 19 January and then much smaller values on 20 and 21 January (McCormick et al., 1982, Table 1). Large extinctions were measured again on 22 January but shifted to the west or at 311˚E. Figure 6 shows the ozone panel for 22 January and the SAM II observation (the solid red dot) over Greenland. It is located in a region of cold temperatures (192 K) and at the western edge of a residual feature near 0˚E in the LIMS ozone. The Aleutian anticyclone intensified by this time and moved the vortex off the Pole. Fig. 6 also shows the locations of profile segments that were screened out of the ozone along the 0˚, 90˚, and 125˚E meridians. In particular, the

LIMS ozone profile segments at 125˚E (white plus marks in Fig. 6) are located in a relatively warm region (~215 to 220 K) and are far above the temperature threshold for PSC formation.

The DIF and RTO ozone thresholds were met 52 and 6 instances, respectively, during 18-22 January. However, there were also 15 instances when the retrieved ozone dropped below 0.2 ppmv and where the retrieved temperatures were often of the order of 200 K or higher (between 14 and 46 hPa). Those instances are considered further with the aid of Figure 7, which shows V6 ozone and temperature from four profiles along an orbit from 118 to 128˚E on 22 January. Three of the four profiles met the ozone screening criteria, while one did not. All four profiles exhibit considerable vertical structure. The RTO threshold was met at 60 hPa for the profile at 73.0˚N, 126.7˚E and was also very nearly met at 41 hPa for the profile at 74.3˚N, 128.3˚E, even though both profiles were far from the DIF threshold. In addition, the retrieved ozone profile at 61.4˚N, 119.5˚E has a mixing ratio of 5.5 ppmv at 19 hPa, but then drops below 0.2 ppmv by 31.6 hPa; screening begins four points higher or at the 19-hPa level, as denoted by the horizontal bar. That ozone profile has a co-located, temperature of 264.2 K at 10 hPa, but then decreases rapidly to 211.8˚K at 31.6 hPa (Fig. 7-solid red curve). Since V6 temperatures have a finite vertical resolution, it is likely that the true atmospheric temperature profile had a vertical gradient even larger. Thus, these V6 temperatures may be biased warm by several degrees at the lower pressure-altitudes of 19 to 31.6 hPa, such that the ozone retrieval algorithm assigns little to no ozone to the tangent layer.

More importantly, the LIMS observations for the orbit along the 125˚E meridian on 22 January were made viewing toward the east and in the direction of the strong horizontal temperature gradient (see Fig. 6). In other words, the line-of-sight geometry for those ascending orbital observations were toward much higher temperatures (see Remsberg et al. (1986), their Fig. 31, to determine the LIMS viewing geometry). Although the V6 algorithm accounts, to first order, for line-of-sight temperature gradients, the calculated LIMS radiances for the nominally, 300-km long, tangent layer are according to a mean Planck blackbody function that is weighted necessarily by the higher temperatures at the far side of the tangent layer. Again, little to no

ozone is required in the tangent layer to achieve a match between the calculated and observed radiances for the retrieval of ozone. The several profiles that were screened out along 118 to 126˚E are "false positives" for PSCs; their ozone mixing ratios dropped below 0.2 ppmv in a region of strong temperature gradients.

Figure 8 shows a number of "false positives" on the plot of temperature for 4 February, or at a time when a large-amplitude, wave-1 forcing had moved the vortex off the Pole. Note that scans screened according to the DIF and/or RTO criteria are not located where the temperature is coldest, but instead where the horizontal temperature gradient is large. In addition, in the middle stratosphere the warmest temperatures are further poleward (not shown), such that vertical temperature gradients are also large from 7 to 31.6 hPa in that region. Because retrieved ozone is sensitive to small biases in temperature, the co-located V6 ozone profiles exhibit, anomalously large vertical gradients that often meet the PSC criteria. While this circumstance leads to false indications of PSCs, their mixing ratios are still spurious. The screening removes them, and they are also not part of the V6 Level 3 product.

5 Occurrences of the effects of PSCs in regions of minimum temperatures

Figure 9 is a time series of the daily occurrences of PSCs between 70˚N and the Pole, based on when the DIF and/or RTO criteria were met (gray circles) and for 15 November through the end of February. Note that often there were multiple scans on a given day that had the signature of PSC effects in ozone and their thresholds occurred for a range of pressure-altitudes (between about 15 to 45 hPa). Those occurrences are related to the daily minimum temperatures for the same latitude band and also as a function of pressure altitude-altitude. The white contour denotes 194 K, and one can see that the effects of PSCs occurred at temperatures just below 192 K, at least in early December and through January. The same threshold criteria were met at warmer temperatures (~196 K or greater) in early February, or when most all of the "false positives" occurred.

Table 1 is a summary of the daily occurrences of PSC effects, as indicated by the DIF criterion, for the region poleward of 45˚N and for the pressure-altitude range of 46.4 to 14.7 hPa. Pressure levels where ozone is first considered free of PSC effects, or PSC_{top}, are listed along with their latitude and longitude locations designated in the Level 2 files "cloud_flags_data_psc" within the archival directory "Data_Screening". Typically, several successive ozone profiles are affected along a given orbit, so average locations and PSC_{top} values were obtained from them for Table 1. Those daily occurrences have been compared with and are found to be similar to those for V5 in Austin et al. (1986, their Table 1). PSC features are found in the V6 ozone from 29 November to 3 December 1978, from 27 December 1978 through 5 January 1979, from 8 January through 23 January 1979, and much less frequently in early February. In general, PSC effects from V6 are found over somewhat smaller geographical areas than from V5, due in part to the fact that the PSC effects of V6 are located more precisely. In addition, the V6 results are based on less conservative screening criteria, instead of being based on an inspection of anomalies in the preliminary, daily mapped ozone fields on pressure surfaces as for V5. Table 1 contains the daily-averaged, upper-level pressures (PSC_{top}), above where perturbations from PSCs are essentially absent in the ozone. For example, the horizontal line on the ozone profile of Fig. 3 for 11 January denotes that location as 19 hPa. The designation, PSC_{top}, is analogous to the parameter cloud top height (CTH), reported for PSCs by Spang et al. (2001; 2005) from the CRISTA-2 and the MIPAS datasets, respectively. Instances where the DIF criterion gave a "false positive" are also provided in that same column of Table 1.

LIMS V6 contains up to 3600 up/down profile pairs for each full day of operations. The LIMS DIF criterion (> 1.7 ppmv) is satisfied in 502 profile pairs across 100 separate orbital segments and between 46.4 and 14.7 hPa through the end of January. Those occurrences represent only 0.22% of all profile pairs for that period. The overall instances of DIF values are 252 (1.7 to 2.0 ppmv), 121 (2.0 to 2.3), 70 (2.3 to 2.6), 32 (2.6 to 2.9), 20 (2.9 to 3.2), and 7 (> 3.2 ppmv). By comparison, the RTO criterion (> 0.7) is met only 20 times, exclusive of DIF, and for the much shorter time of 19 through 31 January. Instances for RTO are 7 (0.7 to 1.0), 5 (1.0 to 1.3), 5 (1.3 to 1.6), and 3 (> 1.6).

According to Figure 9 and Table 1, PSCs developed in late November/early December, dissipated by December 4, and then reformed by late December between 67 and 80˚N and 336 to 50˚E, which is also the region of the cold polar vortex centered near the Greenwich meridian at that time. PSC_{top} values are located between 30 and 21 hPa, but most often near 21 hPa. From 2 to 9 January the region of PSCs expanded and their average top-altitude descended slightly to the 24-hPa level. Then, the vortex and the region of PSCs underwent a westward rotation to near 270˚E (northern Canada) by 11 January. Ozone on that day was screened out within the region of 76±6˚N, 289±41˚E. However, Fig. 3 shows that there was residual contamination from PSCs in several of the adjacent V6 ozone profiles. Thus, ozone remnants are found near where the effects of PSCs are identified, e.g., as in the ozone panels of Figs 2 and 4.

Figure 9 and Table 1 show that PSC_{top} moved downward from 9 to 15 January or between 28 to 36 hPa. On 17 and 18 January new PSCs developed at a higher altitude (17 hPa) over northern Scandinavia or near 0˚E. The major stratospheric sudden warming (SSW) of late January brought much warmer air to the polar region and led to the dissipation of the PSCs. PSC_{top} is distributed in Table 1 in terms of the number of orbits for its sightings at a given pressure value according to occurrences through January: 4 at 14.7 hPa, 3 at 16.7 hPa, 7 at 19.0 hPa, 33 at 21.5 hPa, 6 at 24.5 hPa, 33 at 27.8 hPa, 9 at 31.6 hPa, 4 at 35.9 hPa, and 1 at 40.8 hPa. Most daily PSC_{top} occurrences are at 21.5 hPa (33 sightings) and at 27.8 hPa (33 sightings) with many fewer instances at the intervening level of 24.5 hPa (6 sightings).

Table 1 also contains daily average calculations of relative humidity (RH in %) with respect to ice (List, 1958) in the vicinity of PSC_{top}, based on a nominal water vapor mixing ratio of 6 ppmv and for the T_{min} values occurring in the pressure range of 14.7 and 46.4 hPa. T_{min} is found at the same pressure level as PSC_{top} for a subset of 11 of the 31 days. Those two parameters occurred at the same level most often for 21.5 hPa (4), 24.5 hPa (3), and 31.6 hPa (3). Average T_{min} for those instances is 189.5 K at 21.5 hPa, 190.7 K at 24.5 hPa, and 191.2 K at 31.6 hPa, and the average RH for the set of ten cases is 45%. Thus, the V6 results imply that PSCs formed very close to the altitude of the minimum temperature and at values 2 to 3 K above T_{ICE} and 2 to 3 K

below T_{NAT}. These findings are generally consistent with observed altitudes for the maximum departure of temperature below that of T_{NAT} in Pitts et al. (2011, their Fig. 17a). In addition, Fig. 9 shows that the PSCs were found within a 10-km deep layer. The RH (ice) calculations in Table 1 plus the rather warm and somewhat transient nature of T_{min} indicate that the LIMS-observed, PSCs were more likely due to supercooled ternary solutions (STS) of sulfuric acid, nitric acid, and water or perhaps to hygroscopic, liquid/NAT mixtures (e.g., Pitts et al., 2013; Spang et al., 2016). RH did approach 100% on 17 and 18 January just north of Scandinavia and where the temperature dropped to near 185 K. Those conditions indicate the presence of PSC particles composed of ice, possibly due to effects of ascent and adiabatic cooling following an orographic or synoptic-scale forcing (e.g., Grewe and Dameris, 1997; Carslaw et al., 1998).

While the retrieved LIMS V6 temperatures may be biased a degree or so too warm at pressure-altitudes having significant emissions from PSCs, they would not be biased similarly at and above PSC_{top}, at least away from regions having large temperature gradients. Most researchers have used co-located, re-analysis temperatures from nadir-viewing sensors (like SSU) or from data assimilation models for their interpretations of the formation and maintenance of satellite-observed PSCs (e.g., Hoepfner et al., 2006; Spang et al., 2005; Pitts et al., 2011). Pawson et al. (1999) considered layer-mean temperatures derived from geopotential thicknesses from SSU radiance profiles and compared them with T analyses of the Freie Universität Berlin (FUB) from their network of radiosonde (RAOB) data. They found SSU-RAOB differences that were small and of the order of 1 to 2 K, although they also found that the sign of those differences depended on the vertical gradient of the temperature profile. Typically, the SSU values were a bit higher than the FUB analyses at 50 hPa but lower at 20 to 30 hPa or near PSC_{top}. They attributed that variation with altitude to the relatively low vertical resolution of the SSU measurements (10 km at best) and to a difficulty with allocating any changes in the SSU radiances to equivalent variations of the layer-averaged temperature, at least at the altitude of T_{min}. As noted earlier, LIMS radiances for the retrieval of temperature below the 10-hPa level are based on its CO_2W channel measurements, and they are affected very little by added emissions from a PSC. Thus, one clear advantage of LIMS V6 versus SSU is that LIMS viewed the altitude region of T_{min} more directly; its retrieved temperatures have a vertical resolution of 3.7 km.

6 PSCs from LIMS and SAM II and their co-located temperature, HNO_3, and O_3

Figure 10 (left) is a record of the evolution from 20 November 1978 through 30 January 1979 in terms of the minimum temperature versus longitude at the 550 K level (near 31.6 hPa) for the latitude region of 65 to 70˚N or the domain where SAM II made observations. PSC sightings from the V6 ozone are over plotted as gray circles on this diagram along with the 194 K contour (in the manner of Hovmöller, 1949). In most instances locations of effects of PSCs are within the 194 K contour, which is the nominal threshold temperature at this altitude for the formation of PSCs composed of NAT particles. Locations of observations of PSCs from SAM II are over plotted as black circles, and the LIMS results agree well with them. This finding is an important verification of the locations of PSCs from the LIMS ozone. The LIMS PSCs of 22 and 23 January at 100˚E to 120˚E represent instances, when the RTO threshold was met and when the temperature was well above 194 K. These several cases are false indications of PSCs. Figure 10 (right) shows the corresponding mean HNO_3 at 550 K for the same latitude domain; the white contour is 10 ppbv. PSCs occurred where temperatures (at left) were coldest and often where HNO_3 had its maximum values, and this finding is typical of their anti-correlation in the region of the polar vortex. However, it is also possible that the retrieved HNO_3 was contaminated (high) slightly due to excess emissions from the PSCs themselves.

Figure 11 is analogous to Fig. 10, but for the domain of 70˚N to the Pole and for the period of 25 November through 20 January. The three panels of Fig. 11 are Hovmöller diagrams at 550 K of (left) minimum temperature, (middle) minimum HNO_3, and (right) maximum ozone. Minima and maxima are the min or max values for each longitude as observed between 70N and the pole. The left panel has the LIMS PSCs over plotted in it, and the 194 K contour is shown as a proxy for temperatures that support NAT PSCs. The 10 ppbv HNO_3 contour is shown in white in the middle panel. Maximum ozone is shown in the right panel and highlights remnants of PSCs, as otherwise ozone is always low inside the vortex. Ozone remnants show clearly over the Greenwich Meridian in late November/early December and in late December, and north of

Greenland in middle January. The relatively high max ozone patterns are indicative of the locations of LIMS PSCs.

Figure 11 shows the influence of the Canadian warming of early December on the position of the polar vortex, the reformation of a cold vortex and its embedded PSCs from late December through middle January, and then the development of the warm Aleutian anticyclone and its encroachment into the vortex during late January. The PSC of 6 December near longitude -100˚ is a definite outlier in that it occurs in a region where the local temperature is near 215 K. Even though retrieved ozone drops to zero at 46.4 hPa for that profile, the DIF criterion is met first at the next higher level (40.8 hPa). There is also a large temperature gradient along the tangent layer at that location, so that the PSC feature is considered as a "false positive" like those of 22 and 23 January in Fig 10. In the middle panel one can also see the large values of HNO_3 (12 ppbv) of late autumn, the poleward advection of much lower values to the Pole in early December, the re-establishment of higher values by late December, and then followed by what appears to be a loss of HNO_3 vapor by about 2-3 ppbv just after the re-occurrence of large numbers of PSCs on 9-11 January.

LIMS observed PSC emissions from 29 November through 4 December and then more consistently from 27 December through January. SAM II also made measurements of enhanced extinction on 30 November and 5 January at the low latitude boundary of where LIMS found largest effects in its ozone. The vortex was split on 6 December, following from a so-called "Canadian warming" event. There was a poleward advection of much lower values of HNO_3 from low latitudes to the Pole across the Alaska sector, following that. Those low values show up clearly in Figs. 10 and 11 during the middle of December. PSC effects occurred much more frequently from 2-8 January at about 70 to 80˚N and between 290 and 0˚E and remained nearly stationary. Temperatures in that region were definitely cold enough (<194 K) for the formation of PSCs, and it is very likely that there was some uptake of HNO_3 vapor onto the particles at that time. Still, because that excess emission from the PSCs was also within the center of the vortex it is difficult to distinguish an uptake of the vapor at the same location.

From 8-11 January the character of the vortex underwent a change, such that one can begin to look for a loss of nitric acid vapor downwind of the PSCs. In particular, on 14 January there are PSC remnants in ozone at about 75˚N, 270˚E, having PSC_{top} at 33.4 hPa and a T_{min} of 189.8 K at 21.5 hPa (Table 1). Figure 11 shows that HNO_3 has a maximum of 12 ppbv over Siberia (120˚E) on that date and smaller values (~9 ppbv) at the center of the vortex (0 to 60˚E and ~21.5 km) and where the co-located ozone is only 3 ppmv. Although the relative minimum of HNO_3 of 9 ppbv is equivalent to its values at the middle latitudes, the 3-ppmv ozone is an isolated, absolute minimum for this pressure surface and is representative of its minimum values within the polar vortex. For this reason it is unlikely that the nitric acid of 9 ppbv was the result of advection from lower latitudes, but that it represents qualitative evidence of a loss or an uptake of nitric acid vapor of order 2-3 ppbv onto the PSC particles that are directly upwind and in a region where T is ~192 K.

From 14 to 17 January the Aleutian anticyclone expanded and distorted the vortex, such that the polar low filled at 290˚E but deepened at 110˚E. The region of coldest temperatures shifted to the east. The data of Table 1 indicates that the PSCs of 16 January at 79˚N, 283˚E and at 31.6 hPa were dissipated by 17 January, when new PSCs appeared at 71˚N, 7˚E and at a pressure-altitude of 15.7 hPa. Figure 12 is the 4-panel plot for 17 January, and it characterizes the polar stratosphere during a period of a large number of PSCs (see Fig. 11). In fact, the largest PSC extinction value measured by SAM II occurred on 18 January at 67.7˚N, 22˚E. The polar vortex and its low values of ozone in Fig. 12 are nearly centered over the Pole. White plus symbols indicate the V6 PSCs that were screened out for 17 January, and they occurred in the region of coldest temperatures (~188 to 192 K). Remnants of PSCs are apparent in the panel for ozone just poleward of that. The cyclonic circulation about the vortex transported air parcels eastward from near 290˚E, across the Greenwich meridian, and into the region of coldest temperatures, or just where PSC remnants are indicated by the elevated ozone values. The co-located HNO_3 appears as an isolated region of relatively low values (9 ppbv) in the vicinity of the PSCs and indicates a region of de-nitrification by 2-3 ppbv of the air flowing across the PSC particles. That apparent, temporary uptake of HNO_3 is considered further in the next section.

7 Temperature threshold for the uptake of HNO_3 vapor

Figure 13 is a scatterplot of the minimum levels of HNO_3 versus minimum temperatures at 550 K for the domain of 70˚N to the Pole based on the data in the Hovmöller plots of Fig. 11 (left and middle panels). The temperature threshold of 194 K is marked as the vertical dashed line. Highest values of HNO_3 (10 to 13 ppbv) are found at temperature less than about 198 K and are characteristic of the distribution of HNO_3 in the polar vortex region. It may be that those HNO_3 values also exhibit a slight excess due to contamination from the effects of the PSCs. Yet, Fig. 13 also shows that the range of HNO_3 values is a bit larger (8 to 13 ppbv) for temperatures less than about 196 K. HNO_3 values lower than 10 ppbv imply an uptake of HNO_3 vapor in that domain of colder air.

The points in Figure 13 are also colored by whether the maximum ozone (of the right Hovmöller diagram of Fig. 11) is greater than or less than 6 ppmv. Blue points indicate maximum ozone less than 6 ppmv; red points are where maximum ozone is greater or equal to 6 ppmv and are attributed to PSC effects. All of the red points occur to the left of the dashed black line (indicating < 194 K). Those points span a range of HNO_3 from ~9 to 13 ppbv, and they occurred in middle January. There are also a few red points from mid/late January that are positioned just below them and at temperatures of the order of 188 K. Those points are for a region in the middle panel of Fig. 11 where HNO_3 dips to as low as 8 ppbv.

The above likely uptake of HNO_3 is consistent with findings in the literature from others (Hoepfner et al., 2006; Arnone et al., 2012; Pitts et al., 2013). Such depletion of vapor phase HNO_3 has been shown more clearly from satellite measurements of the Sub Millimeter Radiometer (SMR) and the Microwave Limb Sounder (MLS) (Khosrawi et al., 2011). Still, it is helpful to be able to infer a depletion of the HNO_3 vapor and also to know about the presence and composition of any co-located PSCs. To that end, Hoepfner et al. (1998) found that they could identify PSCs and that the infrared emissions from them amounted to a perturbation of

651 only 2 to 3% in co-located, stratospheric column measurements of HNO_3 vapor. The findings in
652 Fig. 5 show that the effects of PSCs are also small in V6 HNO_3.

653

654 Pitts et al. (2013, their Fig. 2) reported results of their model calculations of the relevant gas-to-
655 particle processes for the uptake of HNO_3 vapor, based on the work of Carslaw et al. (1995) for
656 STS and that of Hanson and Mauersberger (1988) for NAT. They found that significant uptake
657 occurs within a day of so for particles composed of STS, while conversion of vapor onto NAT
658 particles is slower. Yet, they also pointed out that uptake of HNO_3 vapor onto STS particles is
659 only efficient when the environmental temperature is close to T_{ICE}. According to their model,
660 environmental temperatures must be below 189 K at 30 hPa for an uptake of the vapor onto STS
661 droplets. The minimum LIMS temperatures in Table 1 indicate that the STS threshold was
662 achieved on 19 and 20 January. Pitts et al. (2013) also found that that an uptake of 2-3 ppbv of
663 HNO_3 vapor onto NAT particles can occur, when the temperature remains below 193 K for more
664 than 2 to 3 days. Those conditions were met from 5 to 11 January 1979 (Table 1). NAT
665 particles can also form at 50 hPa as temperatures dip below 195 K. However, Fig. 5 shows that
666 the environmental temperature barely met that threshold on 19 January, making any further
667 uptake unlikely at that lower altitude. Detailed trajectory and microphysical calculations are
668 required, in order to obtain more quantitative estimates of the extent and persistence of the local
669 de-nitrification of the air during 1978-1979.

670

671 Solomon et al. (2015) presented several model scenarios for the efficient uptake of HNO_3 vapor
672 and growth of STS particles but only when temperatures drop below 192 K. Their scenarios also
673 required that there be significant supersaturation for the HNO_3 vapor with respect to solid NAT
674 particles or at temperatures also below about 192 K. Based on those assumptions, they also
675 achieved time series of model ozone loss for February and March that agreed well with observed
676 polar ozone changes for the abnormally cold Arctic winter of 2011. By comparison, LIMS
677 temperatures of 192 K or colder did not persist past 24 January, and there is no clear evidence for
678 a corresponding heterogeneous loss of V6 ozone during 1978-1979.

679

8 Seasonal evolution of potential vorticity, HNO_3, and O_3

The previous sections demonstrate that it is important to be aware of the presence of PSC effects in both individual LIMS profiles and in localized regions of the mapped LIMS products. In this section it will be shown that the effects of the remnants of PSCs cover very little area of the northern hemisphere during the winter of 1978/79. First, Figure 14 is a plot of the dynamical tracer, potential vorticity, on the isentropic surface of 550 K (or the IPV at about 31.6 hPa and 22 km) for 17 January.

$$PV = (f + \zeta) / \sigma \quad , \qquad (2)$$

where $f = 2\Omega \sin \varphi$ is the local vertical component of planetary vorticity, $\zeta = \partial v/\partial x - \partial u/\partial y$ is relative vorticity, σ is isentropic density (kg m^{-2} K^{-1}), and $1/\sigma = -g\, \partial\theta/\partial p = (1/\rho)\, \partial\theta/\partial z$ is static stability. Geostrophic wind components, u and v, are calculated at grid points from the LIMS V6 GPH fields. Then, daily values of the vertical component of PV are computed at each grid point from the zonal and meridional components of the wind (u and v), plus the local vertical gradients of potential temperature versus pressure from V6, following Harvey et al. (2009). The white contour denotes the effective edge of the PV vortex, according to the objective criteria of Nash et al. (1996). High values of PV compare favorably with the regions in Fig. 12 of low temperature and geopotential height, low ozone, and high nitric acid. In addition, Fig. 14 shows that there is transport of low PV air toward the Pole near 0˚E and 230˚E; the vortex was distorted and nearly split on 17 January.

Figure 15 is a time series plot of PV at 550 K for 25 October 1978 through 28 May 1979. The ordinate is given in terms of equivalent latitude φ from the Pole (90˚) to 15˚N and is based on a monotonic ordering of the daily LIMS PV from high values inside the polar vortex to low values outside the vortex (e.g., Butchart and Remsberg, 1986). Thus, equivalent latitude is a vortex centered coordinate that assigns the highest PV values (located in the center of the vortex) to be at 90° N. The ordinate is linear in φ to accentuate variations in the PV field at higher equivalent latitudes. Tic marks along the abscissa denote the middle of each month. Time series of the daily data are somewhat noisy (not shown), in part because the LIMS orbital measurements have a repeat cycle over a given latitude and longitude of six days. That sampling pattern means that

only up to 6 zonal waves can be resolved from the data and that the daily character of the actual zonal waves may be aliased slightly (Remsberg et al., 1990). Therefore, a 7-day smoother was applied to the PV time series for Fig. 15 to minimize effects of that sampling bias.

Figure 15 shows clearly that the highest PV value is assigned the highest equivalent latitude; high values occur in midwinter and define the polar vortex. There was an increase of PV at the highest equivalent latitudes from late January and through February, or at the times of the major and then the final SSW events. Highest PV values are also associated with transport through the 550 K surface due to diabatic effects. It is noted that the vortex was split (wave-2) at four separate times at the pressure-altitude of 31.6 hPa: late October, late November/early December, late February, and in early April. Both zonal wave-1 and wave-2 are indicative of the effects of wave forcings as they propagate from the troposphere to the 31.6-hPa level of the stratosphere. Large-scale anticyclones become amplified in winter and dominate the middle latitude stratosphere by springtime; zonal easterlies occur at lower latitudes thereafter. PV gradients were weaker at the mid latitudes by March, and there was erosion of high PV from then onward. That erosion is due to the actions of the large-scale planetary waves, while the adjacent regions of low PV are a result of the meridional mixing of PV from both the lower and higher latitudes (McIntyre and Palmer, 1983).

Nitric acid and ozone are effective tracers of motions in the lower stratosphere; isolines of their mixing ratios ought to be nearly parallel to those of PV. Averages of the HNO_3 and of the ozone values along the PV contours are generated versus φ for each day, as determined for example around a daily PV contour in Fig. 14. Those averages represent approximate, modified Lagrangian means (MLM) of each species at 550 K in the manner of Butchart and Remsberg (1986). The 7-month evolution of the MLM for HNO_3 is displayed in Figure 16, and the contour patterns agree well with those of the PV tracer of Fig. 15. There is little to no indication of any contamination of the HNO_3 due to PSCs on the 550 K surface. Nitric acid varies nearly monotonically in equivalent latitude and attains values near 12 ppbv at the center of the vortex ($\varphi = 90^{\circ}$) upon the approach of winter and in polar night conditions. Such high values indicate a

738 nearly complete chemical conversion of the available NO_y to its reservoir species HNO_3.
739 Poleward of about $\varphi = 60^\circ$ the nitric acid contours are aligned well with those of PV, especially
740 during the winter when further chemical conversions are not effective. The slow accumulation
741 of HNO_3 during the winter at middle equivalent latitudes ($\varphi = 20$ to 45°) indicates that there is
742 significant transport of nitric acid from the polar region at the time of the large-scale zonal wave
743 events. High HNO_3 values that are representative of the polar winter vortex were eroded by
744 early March. Thereafter, HNO_3 decreases at all equivalent latitudes, due to the effects of the
745 chemical re-partitioning of NO_y away from HNO_3 and toward NO_2 in the presence of sunlight.

746

747 The time series of the MLM for ozone is shown in Figure 17, and its isolines deviate appreciably
748 at 550 K from those of PV. From late October to January, lowest values of ozone occur in the
749 vortex, as expected. Relatively low values also occur in the tropics and subtropics for all months
750 and are a result of the slow ascent of the Brewer/Dobson circulation. At about 20-22 January
751 there is a small, isolated region of high apparent ozone at $\varphi = 90^\circ$ or near the center of the PV
752 vortex that is due to the remnants of emissions from PSCs. Note that the high ozone in Fig. 11
753 that occurred near the Greenwich meridian or in the western hemisphere at the end of November,
754 between the end of December and early January, and between 18-20 January is not visible in Fig.
755 17 due to averaging in equivalent latitudes bins. Thus, the prominence of PSC effects in fields of
756 ozone depends on how the data are displayed. Immediately following the time of the major
757 wave-1 warming in late January, lower values of ozone that are characteristic of the center of the
758 vortex are re-established at $\varphi = 90^\circ$. Then, the ozone became larger across most latitudes from
759 late January and until the mid-February final warming. The ozone maximum at middle
760 equivalent latitudes of Fig. 17 differs clearly from the location of the maximum in PV at that
761 time. Daily polar plots for late January/early February (not shown) reveal that, as wave-2
762 increases, the mid-latitude anticyclone moves eastward from the African sector to the Aleutian
763 sector and transports high ozone with it. Thus, higher ozone from lower latitudes is transported
764 poleward as the isolated, Aleutian anticyclone is intensifying (see also Rood et al., 1993). Those
765 regions of high ozone expand further to higher equivalent latitudes by mid-April, following the
766 erosion of the vortex. The hemispheric ozone distributions of Fig. 17 exhibit a steady decline

from mid-April through May, due to the rather slow chemical loss processes that bring ozone back toward its equilibrium state.

Seasonal time series of PV, HNO_3, and ozone at 450 K (~46.4 hPa) are shown in Figures 18-20, respectively. Patterns of PV in Fig. 18 are similar to those at 550 K, except for the smaller magnitudes of the isolines. The meridional gradient of PV is quite weak by midwinter for φ values of 30 to 60˚N, and that character extends to the high latitudes by mid-April or after the air masses have undergone significant meridional mixing. Figure 19 for HNO_3 shows that there are effects from remnants of PSCs at 450 K for several days in mid-January, but the magnitudes of those perturbing effects are small (10 to 15%). Nitric acid values exceed 13 ppbv near φ = 90˚ in late November and early December, but they are typical of values in the polar vortex at that time. Finally, the isolines of ozone from φ = 60 to 90˚ in Figure 20 follow a pattern similar to that of PV, indicating that ozone is an approximate tracer of the seasonal transport at 450 K. Ozone increases at the middle equivalent latitudes from late autumn and through the winter, reflecting an accumulation of ozone in the lower stratosphere. Even though PSC effects tend to be obscured by the averaging of data into equivalent latitude bins, there is an apparent increase in the ozone of Fig. 20 by about 50% from 7-15 January due to remnants of PSCs at φ = 70 to 90˚. There was also transport of lower ozone values from φ = 70 to 85˚ for a week or two thereafter. From late February and onward there is good correspondence between ozone and PV at middle and high equivalent latitudes. Finally, while the meridional gradients for ozone are much weaker than for HNO_3 near φ = 65˚, their respective seasonal patterns remain similar to those of PV.

9 Conclusions

The primary findings about the occurrences of PSCs from the LIMS V6 dataset are similar in many respects to those from the LIMS V5 data in Austin et al. (1986), who reported that the occasional Arctic PSC signatures occurred at temperatures less than 194 K but above the saturation point with respect to water ice. Locations of the PSC signatures are determined more precisely with the V6 data because the V6 radiances were conditioned for instrument effects more carefully and the V6 retrievals for temperature and species were processed for every pair of

796 profiles along the orbit. The resulting V6 profile points are also provided at more levels (at
797 every 0.88 km in altitude). Two criteria were applied to automate and objectify the detection of
798 effects of PSCs in the V6 ozone profiles. The primary criterion for sensing effects of PSCs is
799 based on an increase of the retrieved ozone mixing ratio by at least 1.7 ppmv over a decrease in
800 altitude of 0.88 km; that DIF criterion accounted for 96% of PSC sightings in the pressure range
801 of 14.7 to 46.4 hPa. Profile segments that met the DIF threshold were screened from all the
802 LIMS species. The remaining 4% of instances are due to the ozone exceeding a ratio criterion
803 (RTO) that may also be triggered due to normal, dynamically-induced structures in the profiles.
804 In fact, the RTO criterion was met more frequently at the lower levels of 52 to 100 hPa. During
805 the testing of the screening criteria, it was found that tighter thresholds indicated more instances
806 of PSC-like effects but also triggered the removal of more profile segments having vertical ozone
807 structures in regions where the environmental temperatures were much too warm for the
808 formation and maintenance of PSCs.

809

810 The retrieved V6 temperature profiles were not screened, even though the co-located temperature
811 profiles may be a degree or so too warm at the altitude of maximum perturbing effects from
812 PSCs in the ozone. On the other hand, there is no evidence for a temperature bias at and above
813 tops of PSCs. Minimum temperature values most often occurred just above tops of PSCs and
814 with values between about 187 K and 192 K. Such threshold temperatures indicate that the PSCs
815 were composed of STS and NAT aerosols. The altitude range for the occurrence of tops of
816 Arctic PSCs was from 21 to 28 hPa, on average, although there was a tendency for the PSCs to
817 descend within the winter polar vortex over time in 1978-1979. Temperature and geopotential
818 height profiles and the LIMS Level 3 zonal coefficients derived from the mapping of them are
819 judged as appropriate for calculations of stratospheric transport. Based on the findings of the
820 analyses from LIMS V6, it is recommended that future stratospheric, limb-infrared ozone
821 experiments ought to include a separate channel(s) for the detection of PSC/aerosol emissions, in
822 order to screen out or to make first-order corrections for their effects in retrievals of ozone and
823 other trace species (e.g., see Spang et al., 2016). In addition, the instruments ought to include a

824 wide-band, 15-μm CO_2 channel that is nearly insensitive to PSC/aerosol emissions, so that co-
825 located temperature profiles are also available with little to no bias.

826

827 The LIMS V6 rather than V5 data are more compatible with stratospheric datasets from recent
828 satellite experiments. It is primarily for this reason that the V6 data have been included as part
829 of the SPARC-Data Initiative. Although a small fraction of the V6 ozone, H_2O, and NO_2
830 profiles may contain remnants of the effects of emissions from PSCs, the co-located, LIMS-
831 retrieved HNO_3 profiles are affected much less. Remnants of the effects of PSCs are found in
832 the V6 ozone and HNO_3 in mid-January and at equivalent latitudes poleward of 70˚. An initial
833 look was given to the distributions of the V6 nitric acid and co-located temperatures. It is
834 concluded that there was a qualitative uptake of nitric acid vapor and a temporary de-nitrification
835 of the air by about 2-3 ppbv just downwind of PSCs during mid-January and in the region of the
836 polar vortex where the temperatures were at or below 194 K.

837

838 Seasonal time series of both ozone and HNO_3 indicate significant meridional transport of the air
839 about the vortex and between the middle latitudes and the Pole, associated with the zonal wave-1
840 events of early December and of 14 to 27 January. In particular, there is a good correspondence
841 for the time series of ozone and nitric acid vapor with that of potential vorticity on the 450 K
842 (~46.4 hPa) potential temperature surface. During late autumn and early winter both those
843 species are also excellent tracers of the transport and mixing at 550 K (~31.6 hPa). But by
844 March it is clear that there was a significant accumulation of ozone at middle and higher
845 equivalent latitudes at 550 K. It is also concluded that the V6 data provide accurate, associated
846 temperature and GPH fields for conducting transport studies of that time period.

847

Acknowledgements. The authors (EER and VLH) are grateful to R. Earl Thompson and to John Burton, B. Thomas Marshall, Praful Bhatt, Mark Melbert, and Larry Gordley for testing the LIMS V6 cloud and PSC detection algorithms and for processing the Level 2 dataset, respectively. Gretchen Lingenfelser generated the LIMS V6 Level 3 product that is archived at NASA Goddard Space Flight Center (GES DISC). The V6 dataset is archived at the Goddard Earth Sciences Data and Information Services Center (GES DISC and its Website: daac.gsfc.nasa.gov) and is accessible for scientific use via ftp download. The analyses herein have been motivated by an inquiry to the LIMS Science Team in 1986 from Paul Crutzen, who was hoping to find instances of nitric acid uptake using the LIMS V5 dataset. The authors acknowledge, Lamont Poole, who carried out some specific calculations with his model, showing the likelihood of nitric acid uptake for the conditions of the 1978-1979 Arctic winter. They relied on his results as a check on the conclusions herein about nitric acid uptake onto STS and NAT particles. VLH acknowledges support from NASA LWS Grant NNX14AH54G and NSF CEDAR AGS Grant 0940124. EER carried out his work while serving as a Distinguished Research Associate within the Science Directorate at NASA Langley.

References

Arnone, E., Castelli, E., Papandrea, E., Carlotti, M., and Dinelli, B. M.: Extreme ozone depletion in the 2010-20111 Arctic winter stratosphere as observed by MIPAS/ENVISAT using a 2-D tomographic approach, Atmos. Chem. Phys., 12, 9149-9165, doi:10.5194/acp-12-9149-2012, 2012.

Austin, J., Remsberg, E. E., Jones, R. L., and Tuck, A. F.: Polar stratospheric clouds inferred from satellite data, Geophys. Res. Lett., 13, 1256-1259, 1986.

Brasseur, G. P, and Solomon, S.: Aeronomy of the middle atmosphere, 3rd Edition, Springer, The Netherlands, 644 pp., 2005.

Butchart, N., and Remsberg, E. E.: The area of the stratospheric polar vortex as a diagnostic for tracer transport on an isentropic surface, J. Atmos. Sci., 43, 1319-1339, 1986.

Carslaw, K. S., Luo, B. P., and Peter, T.: An analytic expression for the composition of aqueous HNO_3-H_2SO_4 stratospheric aerosols including gas phase removal of HNO_3, Geophys. Res. Lett., 22, 1877-1880, 1995.

Carslaw, K. S., Wirth, M., Tsias, A., Luo, B. P., Dörnbrack, A., Leutbecher, M., Volkert, H., Renger, W., Bacmeister, J. T., and Peter, T.: Particle microphysics and chemistry in remotely observed mountain polar stratospheric clouds, J. Geophys. Res., 103, D5, 5785-5796, 1998.

Crutzen, P. J., and Arnold, F.: Nitric acid cloud formation in the cold Antarctic stratosphere: a major cause for the springtime 'ozone hole', Nature, 324, 651-655, 1986.

Gille, J. C., and Russell III, J. M.: The limb infrared monitor of the stratosphere: experiment description, performance, and results, J. Geophys. Res., 89, 5125-5140, 1984.

Grewe, V., and Dameris, M.: Heterogeneous PSC ozone loss during an ozone mini-hole, Geophys. Res. Lett., 24, 2503-2506, 1997.

Hamill, P., and McMaster, L. R., Eds.: Proceedings of a workshop on polar stratospheric clouds, their role in atmospheric processes, NASA/CR-2318-19840024881, available at http://www.sti.nasa.gov (last access: 6 May 2015), 79 pp., 1984.

Hanson, D., and Mauersberger, K.: Laboratory studies of the nitric acid trihydrate: implications for the south polar stratosphere, Geophys, Res. Lett.., 15, 855-858, 1988.

Harvey, V. L., Randall, C. E., and Hitchman, M. H.: Breakdown of potential vorticity-based equivalent latitude as a vortex-centered coordinate in the polar winter mesosphere, J. Geophys. Res., 114, D22105, doi:10.1029/2009JD012681, 2009.

Hoepfner, M., Blom, C. E., Fischer, H., Glatthor, N., Gulde, T., Piesch, C., Renger, W., and Wirth, M.: HNO_3 and PSC measurements from the TRANSALL: sequestering of HNO_3 in the winter of 1994/95, J. Atmos. Chem., 30, 61-79, 1998.

Hoepfner, M., Luo, B. P., Massoli, P., Cairo, F., Spang, R., Snels, M., Di Donfrancesco, G., Stiller, G., von Clarmann, T., Fischer, H., and Biermann, U.: Spectroscopic evidence for NAT, STS, and ice in MIPAS infrared limb emission measurements of polar stratospheric clouds, Atmos. Chem. Phys., 6, 1201-1219, 2006.

915 Hovmöller, E.: The trough-and-ridge diagram, Tellus, 1(2), 62-66, 1949.

916

917 Khosrawi, F., Urban, J., Pitts, M. C., Voelger, P., Achtert, P., Kaphlanov, M., Santee, M. L.,
918 Manney, G. L., Murtagh, D., and Fricke, K.-H.: Denitrification and polar stratospheric cloud
919 formation during the Arctic winter 2009/2010, Atmos. Chem. Phys., 11, 8471-8487,
920 doi:10.5194/acp-11-8471-2011, 2011.

921

922 Knudsen, B. M.: Accuracy of arctic stratospheric temperature analyses and the implications for
923 the prediction of polar stratospheric clouds, Geophys. Res. Lett., 23, 3747-3750, 1996.

924

925 Leovy, C. B., Sun, C-R., Hitchman, M. H., Remsberg, E. E., Russell III, J. M., Gordley, L. L.,
926 Gille, J. C., and Lyjak, L. V.: Transport of ozone in the middle stratosphere: evidence for
927 planetary wave breaking, J. Atmos. Sci., 42, 230-244, 1985.

928

929 List, R. J.: Smithsonian Meteorological Tables, Smithsonian Institute, Washington, DC, 1958.

930

931 McCormick, M. P., Steele, H. M., Hamill, P., Chu, W. P., and Swissler, T. J.: Polar stratospheric
932 cloud sightings by SAM II, J. Atmos. Sci., 39, 1387-1397, 1982.

933

934 McIntyre, M. E., and Palmer, T. N.: Breaking planetary waves in the stratosphere, Nature, 305,
935 593-600, 1983.

936

937 Nash, E. R., Newman, P. A., Rosenfield, J. E., and Schoeberl, M. R.: An objective determination
938 of the polar vortex using Ertel's potential vorticity, J. Geophys. Res., 101, 9471-9478, 1996.

939

940 Pawson, S., Krueger, K., Swinbank, Bailey, M., and O'Neill, A.: Intercomparison of two
941 stratospheric analyses: temperatures relevant to polar stratospheric cloud formation, J. Geophys.
942 Res., 104 (D2), 2041-2050, 1999.

943

944 Pitts, M. C., Poole, L. R., Dörnbrack, A., and Thomason, L. W.: The 2009-2010 Arctic polar
945 stratospheric cloud season: a CALIPSO perspective, Atmos. Chem. Phys., 11, 2161-2177,
946 doi:10.5194/acp-11-2161-2011, 2011.

947

948 Pitts, M. C., Poole, L. R., Lambert, A., and Thomason, L. W.: An assessment of CALIOP polar
949 stratospheric cloud composition classification, Atmos. Chem. Phys., 13, 2975-2988,
950 doi:10.5194/acp-13-2975-2013, 2013.

951

952 Remsberg, E., and Lingenfelser, G.: LIMS Version 6 Level 3 dataset, NASA/TM-2010-216690,
953 available at http://www.sti.nasa.gov (last access: 6 May 2015), 13 pp., 2010.

954

955 Remsberg, E. E., Kurzeja, R. J., Haggard, K. V., Russell III, J. M., and Gordley, L. L.:
956 Description of data on the Nimbus 7 LIMS map archive tape—ozone and nitric acid, NASA/TP-
957 1986-2625, available at http://www.sti.nasa.gov (last access: 6 May 2015), 71 pp., 1986.

958

959 Remsberg, E. E., Haggard, K. V., and Russell III, J. M.: Estimation of synoptic fields of middle
960 atmosphere parameters from Nimbus-7 LIMS profile data, J. Atmos. Oceanic Tech., 7, 689-705,
961 1990.

962

963 Remsberg, E. E., Gordley, L. L., Marshall, B. T., Thompson, R. E., Burton, J., Bhatt, P., Harvey,
964 L. V., Lingenfelser, G., and Natarajan, M.: The Nimbus 7 LIMS version 6 radiance conditioning

965 and temperature retrieval methods and results, J. Quant. Spectros. Rad. Transf., 86, 395-424,
966 doi:10.1016/j.jqsrt.2003.12.007, 2004.

967

968 Remsberg, E., Lingenfelser, G., Natarajan, M., Gordley, L., Marshall, B. T., and Thompson, E.:
969 On the quality of the Nimbus 7 LIMS version 6 ozone for studies of the middle atmosphere, J.
970 Quant. Spectros. Rad. Transf., 105, 492-518, doi:10.1016/j.jqsrt.2006.12.005, 2007.

971

972 Remsberg, E., Natarajan, M., Marshall, B. T., Gordley, L. L., Thompson, R. E., and
973 Lingenfelser, G.: Improvements in the profiles and distributions of nitric acid and nitrogen
974 dioxide with the LIMS version 6 dataset, Atmos. Chem. Phys., 10, 4741-4756, doi:10.5194/acp-
975 10-4741-2010, 2010.

976

977 Rood, R. B., Douglass, A. R., Kaye, J. A., and Considine, D. B.: Characteristics of wintertime
978 and autumn nitric acid chemistry as defined by limb infrared monitor of the stratosphere (LIMS)
979 data, J. Geophys. Res., 98, D10, 18,533-18,545, 1993.

980

981 Schlager, H., and Arnold, F.: Measurements of stratospheric gaseous nitric acid in the winter
982 Arctic vortex using a novel rocket-borne mass spectrometric method, Geophys. Res. Lett., 17,
983 433-436, 1990.

984

985 Solomon, S., Kinnison, D., Bandora, J., and Garcia, R.: Simulation of polar ozone depletion: an
986 update, J. Geophys. Res., doi:10.1002/2015JD023365, 2015.

987

988 Spang, R., Riese, M., and Offermann, D.: CRISTA-2 observations of the south polar vortex in
989 winter 1997: a new dataset for polar process studies, Geophys. Res. Lett., 28, 3159-3162, 2001.

990

Spang, R., Remedios, J. J., Kramer, L. J., Poole, L. R., Fromm, M. D., Mueller, M., Baumgarten, G., and Konopka, P.: Polar stratospheric cloud observation by MIPAS on ENVISAT: detection method, validation and analysis of the northern hemisphere winter 2002/2003, Atmos. Chem. Phys., 5, 679-692, 2005.

Spang, R., Hoffmann, L., Hoepfner, M., Griessbach, S., Müller, R., Pitts, M. C., Orr, A. M. W., and Riese, M.: A multi-wavelength classification method for polar stratospheric cloud types using infrared limb spectra, Atmos. Meas. Tech. Discuss., doi:10.5194/amt-2016-20, 2016.

Tegtmeier, S., Hegglin, M. I., Anderson, J., Bourassa, A., Brohede, S., Degenstein, D., Froidevaux, L., Fuller, R., Funke, B., Gille, J., Jones, A., Kasai, Y., Krüger, K., Kyrölä, E., Lingenfelser, G., Lumpe, J., Nardi, B., Neu, J., Pendlebury, D., Remsberg, E., Rozanov, A., Smith, L., Toohey, M., Urban, J., von Clarmann, T., Walker, K. A., Wang, R. H. J.: SPARC Data Initiative: A comparison of ozone climatologies from international satellite limb sounders, J. Geophys. Res., 118, 12,229–12,247, doi:10.1002/2013JD019877, 2013.

WMO (World Meteorological Organization): Scientific assessment of ozone depletion: 2014, Global Ozone Research and Monitoring Project, Report No. 55, Geneva, Switzerland, 2014.

1010

Date	Lat˚N	Long˚E	PSC (top), hPa; # DIF	Minimum Temp, K	P (hPa) at T min	RH wrt Ice (%)
11/29	74±2	0±2	22, 3	188.6	24.5	58
11/30	72±5	23±6	22, 13	188.8	21.5	49
12/1	71±3	45±5	32, 9	190.2	31.6	57
12/2	73±3	12±28	22, 5	190.4	21.5	38
12/3	71	8	22, 1	191.5	16.7	24
12/27	76	4	28, 1	192.1	19.0	25
12/28	76±3	356±20	22, 8	190.5	21.5	37
12/30	76±4	352±14	25, 8	190.7	21.5	36
1/1	70±4	359±17	22, 9	191.0	27.8	44
1/2	73±5	332±42	25, 31	190.2	24.5	44
1/3	70±6	340±50	25, 36/1	190.5	24.5	42
1/4	67±6	348±36	25, 19	191.4	24.5	36
1/5	73±3	22±3	32, 7	191.8	31.6	44
1/8	79±4	333±43	22, 27	189.5	24.5	50
1/9	76±8	335±55	28, 78	189.3	24.5	52
1/10	77±7	312±68	28, 78	189.9	24.5	47
1/11	76±6	289±41	28, 52	189.8	21.5	42
1/13	75±9	273±31	28, 26	190.2	21.5	39
1/14	74±8	270±9	32, 11	189.9	21.5	41
1/15	77±2	276±19	36, 5	191.0	21.5	34
1/16	79±2	283±19	32, 3	191.4	21.5	32
1/17	71±5	7±17	17, 11	185.7	24.5	97
1/18	70±7	31±16	17, 21	186.3	27.8	99
1/19	65±8	45±13	22, 15	188.1	21.5	56

1/20	57±4	50±1	15, 6	187.5	14.7	42
1/21	55±3	91±21	32, 3/2	191.7	31.6	44
1/22	65±5	47±47	17, 7/5	190.1	21.5	40
1/23	65±2	359±14	28, 5/1	192.0	27.8	37
2/2	74	52	28, 3/1	196.5	40.8	26
2/3	76	78	19, 6/5	197.2	35.9	21
2/4	73	70±1	27, 23/21	196.4	46.4	30
2/5	81±2	75 & 125	27, 29/27	196.9	40.8	25
2/6	82±1	80 & 112	27, 38/36	195.8	46.4	34
2/7	78	70	32, 18/17	197.7	46.4	25
2/9	76±1	92±2	36, 4/2	196.4	40.8	27

Table 1—Occurrences of signatures of PSCs in the LIMS V6 ozone profiles of 1978/79. Central latitude and longitude locations of the PSCs and their extent (± in degrees) are given for each day that they are found along with the average pressure level (in hPa) at which those perturbing effects are absent, or PSC_{top}, for pressure levels between 14.7 and 46.4 hPa. The number of profiles where the DIF threshold was met is indicated to the right in the column for PSC_{top}., and the number of "false positives" is given to the right of the slash symbol (e.g,, three scans met the DIF criterion on 2 February and one of those was a "false positive" denoted as 3/1). The minimum temperature in the set of profiles and its pressure level is given in the next column. Calculated relative humidity (RH in %) with respect to ice is in the last column, based on an ambient water vapor mixing ratio of 6.0 ppmv.

Figure legends

Figure 1—LIMS V5 ozone mixing ratio profile at 68˚N, 258˚E on 11 January 1979, showing effects of uncorrected emissions from PSCs below about the 20-hPa level.

Figure 2— Polar orthographic projections of Northern Hemisphere ozone (top left), geopotential height (gph, top right), temperature (bottom left), and nitric acid vapor (bottom right) for 11 January 1979 at 31.6 hPa; successive latitude circles are at every 10˚. The Greenwich meridian extends horizontally to the right. Contour intervals are every 0.75 ppmv for ozone, 0.25 km for gph, 4 K for temperature, and 1 ppbv for nitric acid vapor. White plus signs denote orbital profile segments that were screened out; red dot denotes location of SAM II PSC observation.

Figure 3—(at right) Five successive LIMS V6 ozone profile segments along an orbital tangent path from 63˚N to 68˚N and at 259±1˚E on 11 January 1979. The profile at 68.4˚N, 258.2˚E underwent a screening for contamination from effects of emissions from PSCs (below short horizontal line at the 19-hPa level); (at left) temperature profile segments (in red) co-located with the two ozone profiles at 68.4˚N and 64.5˚N.

Figure 4—As in Fig. 2 for 11 January, but for the 46.4-hPa level; the white plus signs have been removed to give better clarity for the underlying fields.

Figure 5—Profiles of LIMS V6 nitric acid vapor (at right) and two co-located profiles of temperature (at left) for 11 and 19 January. Horizontal line at 19 hPa marks the cutoff level for valid nitric acid on 11 January and at 68.4˚N, 258.2˚E.

Figure 6—As in Fig. 2, but for 22 January 1979.

Figure 7—(at right) Four ozone profile segments along an orbital tangent path from 61.4˚N to 74.3˚N and 119.5˚E to 128.3˚E on 22 January 1979 and where short horizontal lines denote the lower altitude limit of good data; (at left) temperature profiles (in red) co-located with the ozone.

Figure 8—V6 temperatures at 31.6 hPa and the locations of spurious PSC effects (white plus signs) for 4 February 1979.

Figure 9—Daily time series of minimum V6 temperatures versus pressure-altitude for the latitude zone of 70˚N to the Pole, plus locations of tops of PSCs (gray circles). Contour increment is 2 K and the white contour is 194 K. The abscissa is from 15 November through 28 February.

Figure 10—Hovmöller diagram (time vs. longitude) of the effects of PSCs from LIMS V6 (gray circles) and from SAM II (black circles) for 20 November 1978 to 30 January 1979. (left) Locations of PSC sightings are over plotted on fields of daily mean temperature between 65-70˚N; contour interval is 2.5 K and the white contour is 194 K. (right) The fields are of daily mean HNO_3; contour interval is 0.5 ppbv and white contour is 10 ppbv.

Figure 11—As in Fig. 10, but for the latitude domain of 70˚N to the Pole and from 25 November through 20 January; (left) fields of daily minimum temperature, (middle) daily minimum HNO_3, and (right) daily maximum ozone.

Figure 12—As in Fig. 2, but for 17 January.

Figure 13—Scatterplot of minimum values of HNO_3 versus minimum values of temperature for the domain of 70˚N to the Pole at 550 K (from Figure 11); the vertical dashed line denotes 194

K. The corresponding maximum values of ozone are shown as red (> 6 ppmv) versus blue (<6 ppmv).

Figure 14—Isentropic potential vorticity (PV) at 550 K for 17 January 1979. Units of PV are in terms of (10^{-6} m^2 s^{-1} K kg^{-1}), and contour interval (CI) is 7 units. The thick white contour denotes the polar vortex edge as defined using Nash et al. (1996).

Figure 15—Time series of LIMS isentropic PV versus equivalent latitude at 550 K and with smoothing over 7 days. PV contour interval (CI) is 10 units.

Figure 16—As in Fig. 15, but for HNO_3 (CI is 0.5 ppbv).

Figure 17—As in Fig. 15, but for ozone (CI is 0.2 ppmv).

Figure 18—As in Fig. 15, but for PV versus equivalent latitude at 450 K (CI is 3.2 units).

Figure 19—As in Fig. 16, but for HNO_3 at 450 K (CI is 0.5 ppbv).

Figure 20—As in Fig. 17, but for ozone at 450 K (CI is 0.25 ppmv).

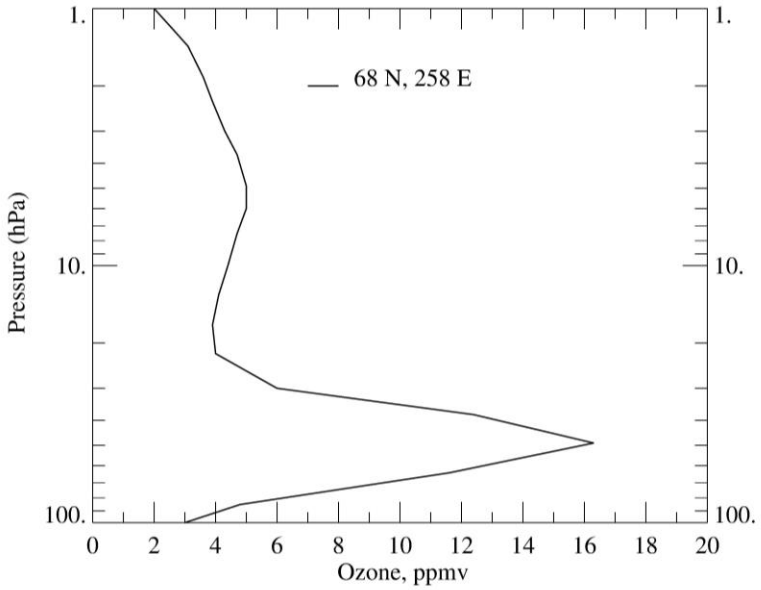

1097

1098 Figure 1—LIMS V5 ozone mixing ratio profile at 68˚N, 258˚E on 11 January 1979, showing
1099 effects of uncorrected emissions from PSCs below about the 20-hPa level.

1100

1101

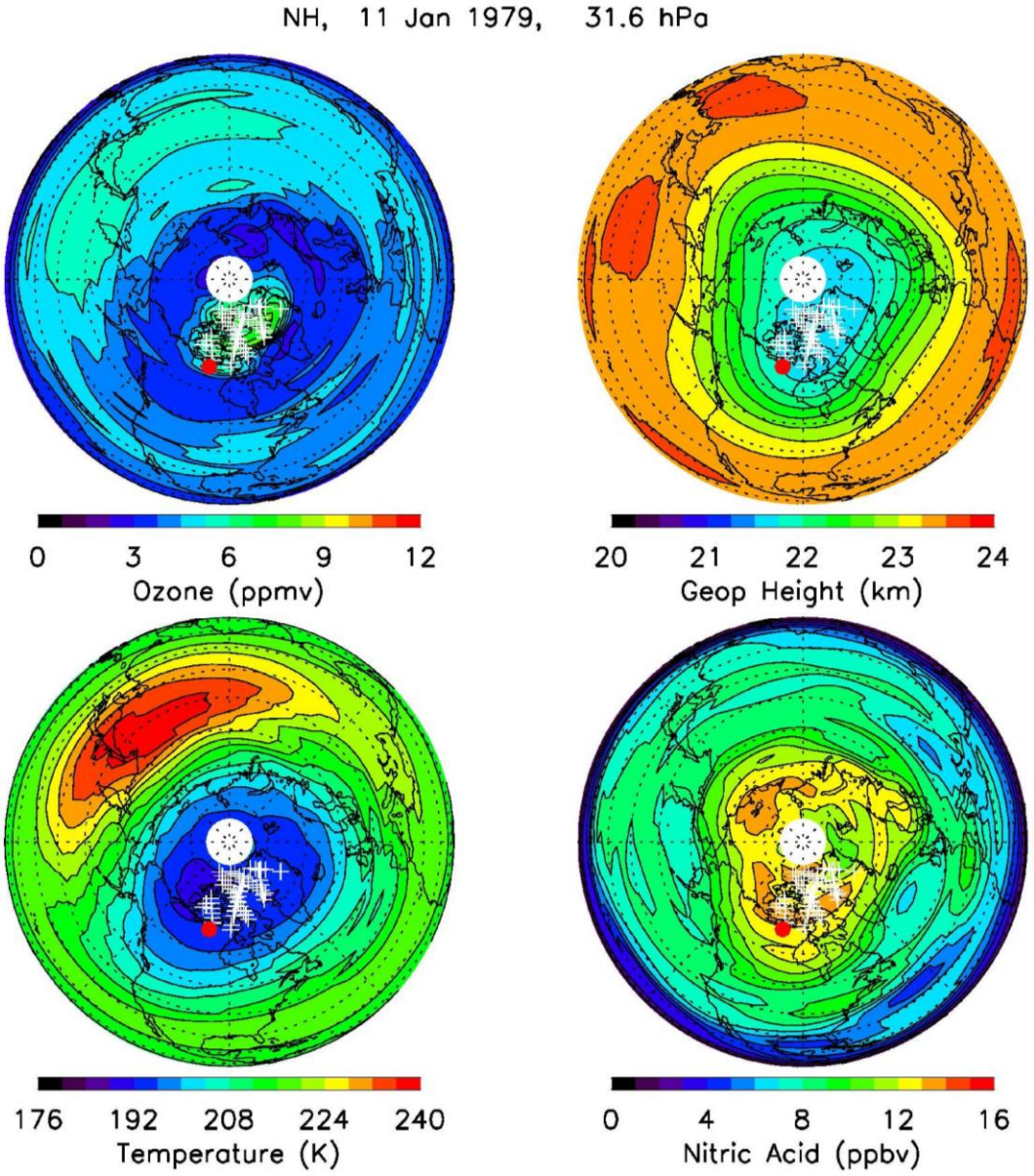

Figure 2— Polar orthographic projections of Northern Hemisphere ozone (top left), geopotential height (gph, top right), temperature (bottom left), and nitric acid vapor (bottom right) for 11 January 1979 at 31.6 hPa; successive latitude circles are at every 10˚. The Greenwich meridian extends horizontally to the right. Contour intervals are every 0.75 ppmv for ozone, 0.25 km for gph, 4 K for temperature, and 1 ppbv for nitric acid vapor. White plus signs denote orbital profile segments that were removed; red dot denotes location of SAM II PSC observation.

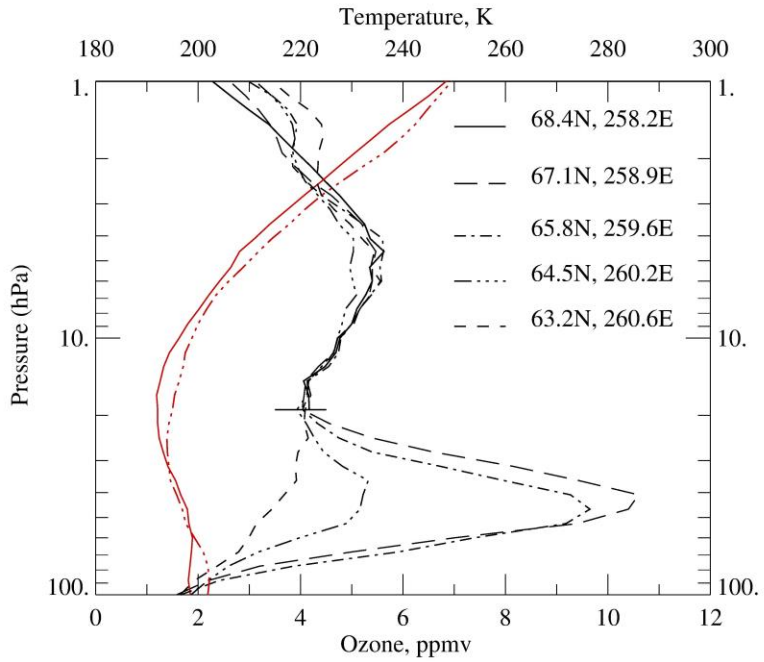

1110

1111 Figure 3—(at right) Five successive LIMS V6 ozone profile segments along an orbital tangent
1112 path from 63˚N to 68˚N and at 259±1˚E on 11 January 1979. The profile at 68.4˚N, 258.2˚E
1113 underwent a screening of contamination from effects of emissions from PSCs (below short
1114 horizontal line at the 19-hPa level); (at left) temperature profile segments (in red) co-located with
1115 the two ozone profiles at 68.4˚N and 64.5˚N.

1116

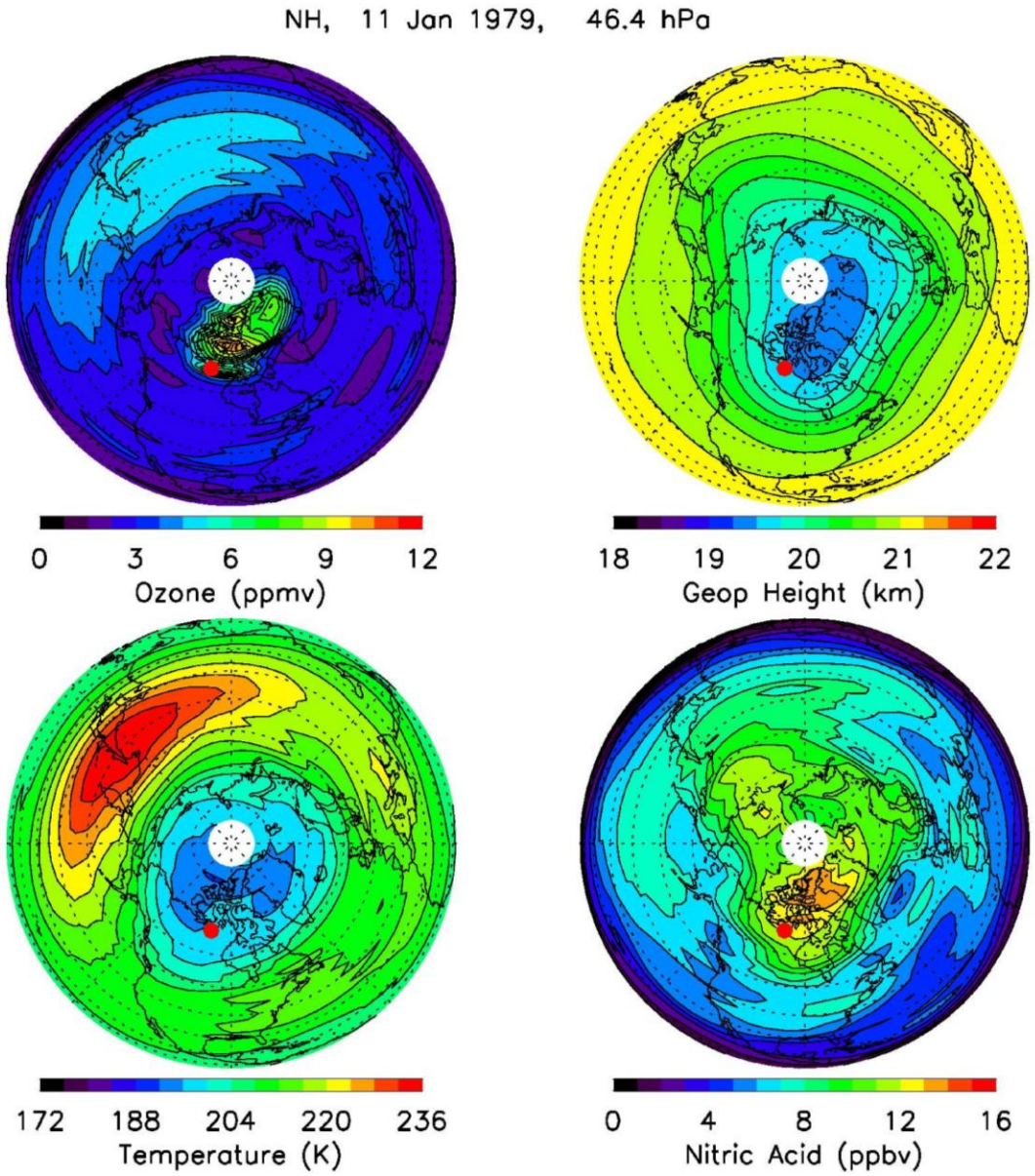

1117

1118 Figure 4—As in Fig. 2 for 11 January, but for the 46.4-hPa level; the white plus signs have been
1119 removed to give better clarity for the underlying fields.

1120

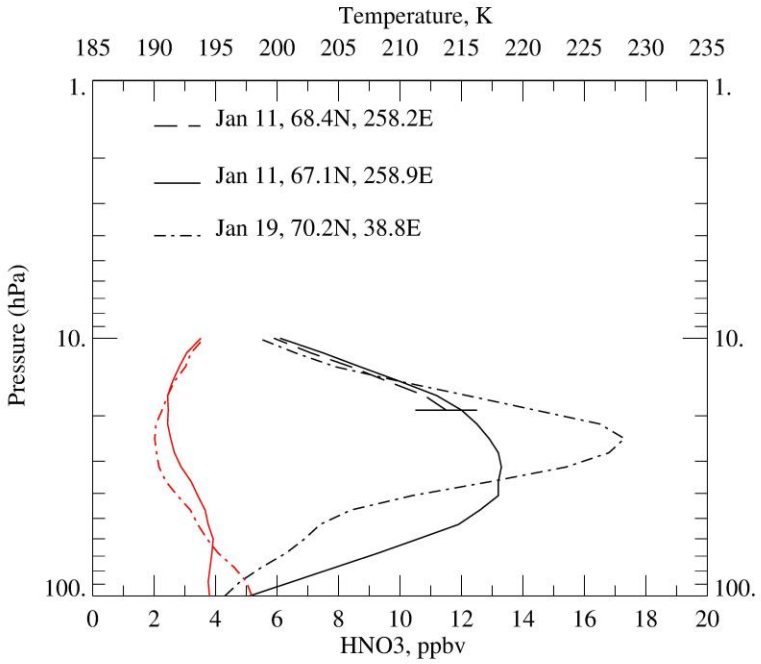

Figure 5—Profiles of LIMS V6 nitric acid vapor (at right) and two co-located profiles of temperature (at left) for 11 and 19 January. Horizontal line at 19 hPa marks the cutoff level for valid nitric acid on 11 January and at 68.4˚N, 258.2˚E.

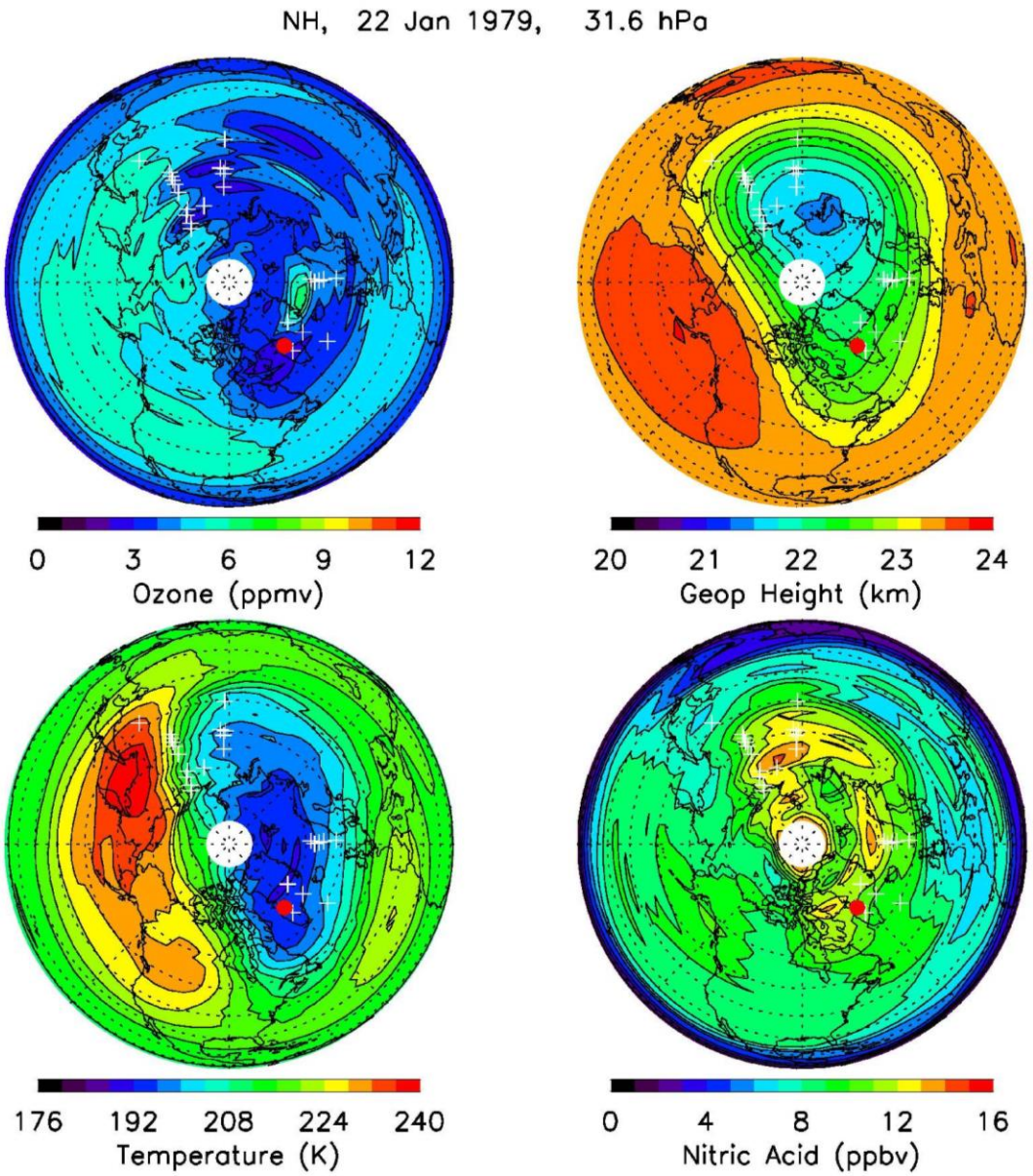

Figure 6—As in Fig. 2, but for 22 January 1979.

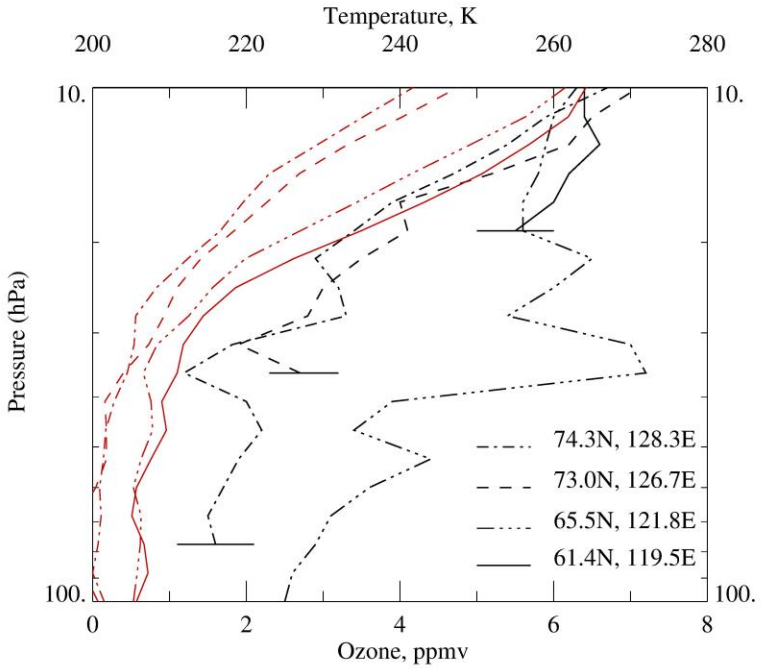

Figure 7—(at right) Four ozone profile segments along an orbital tangent path from 61.4˚N to 74.3˚N and 119.5˚E to 128.3˚E on 22 January 1979 and where short horizontal lines denote the lower altitude limit of good data; (at left) temperature profiles (in red) co-located with the ozone.

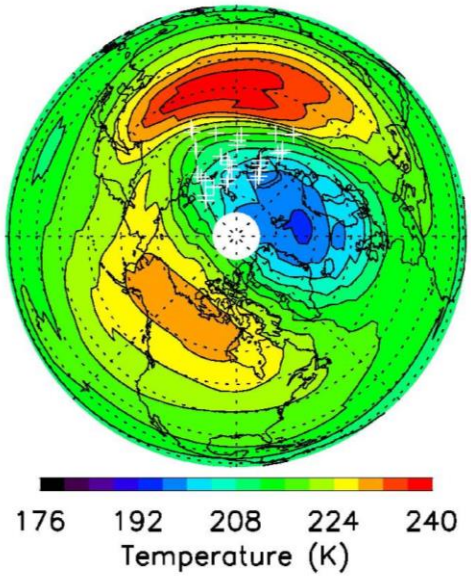

Figure 8—V6 temperatures at 31.6 hPa and the locations of spurious PSC effects (white plus signs) for 4 February 1979.

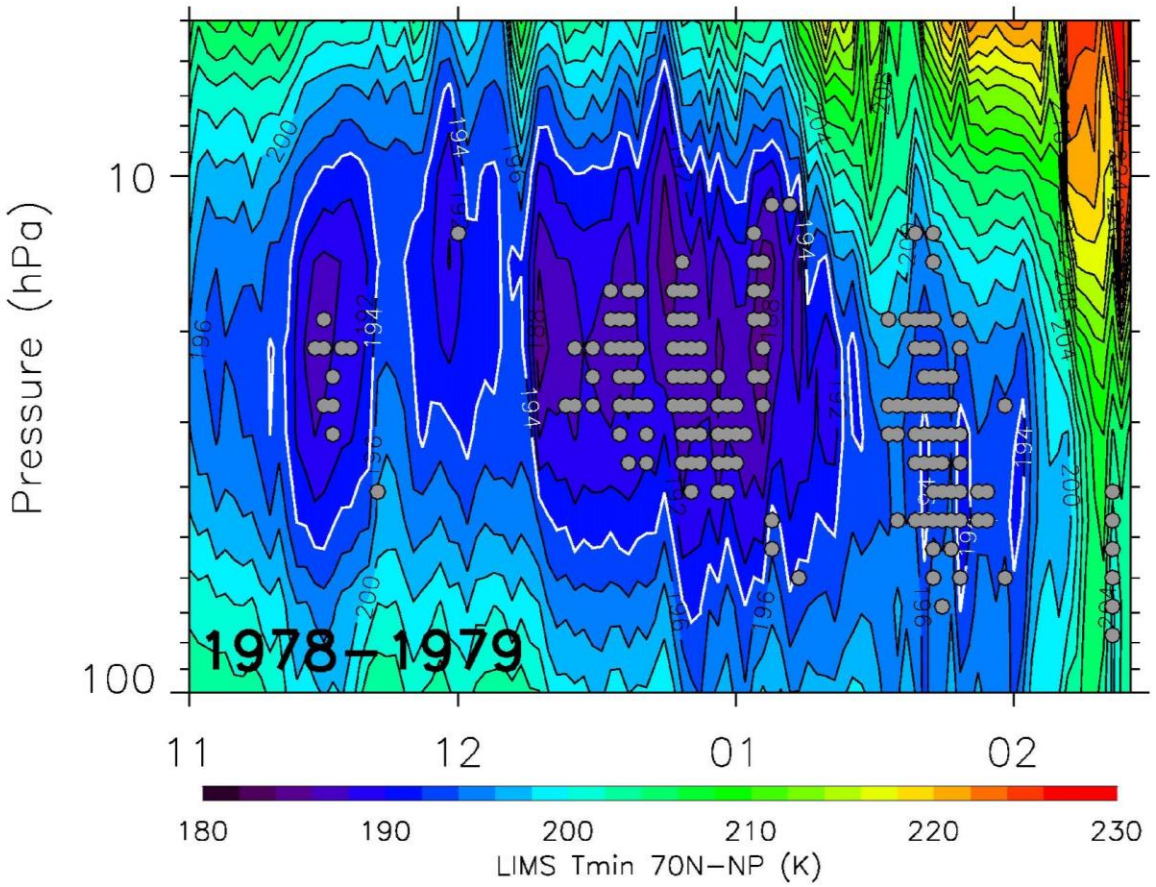

Figure 9—Daily time series of minimum V6 temperatures versus pressure-altitude for the latitude zone of 70˚N to the Pole, plus locations of tops of PSCs (gray circles). Contour increment is 2 K and the white contour is 194 K. The abscissa is from 15 November through 28 February.

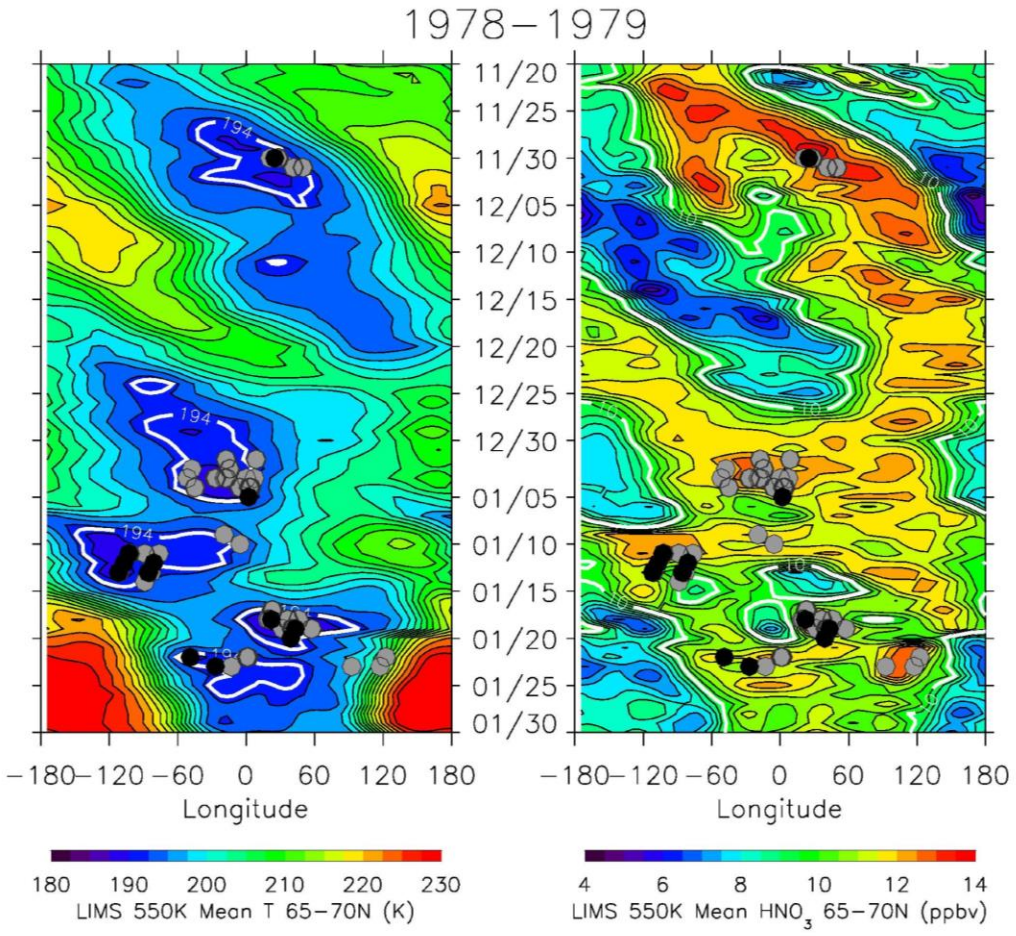

Figure 10— Hovmöller diagram (time vs. longitude) of the effects of PSCs from LIMS V6 (gray circles) and from SAM II (black circles) for 20 November 1978 to 30 January 1979. (left) Locations of PSC sightings are over plotted on fields of daily mean temperature between 65-70˚N; contour interval is 2.5 K and the white contour is 194 K. (right) The fields are of daily mean HNO_3; contour interval is 0.5 ppbv and white contour is 10 ppbv.

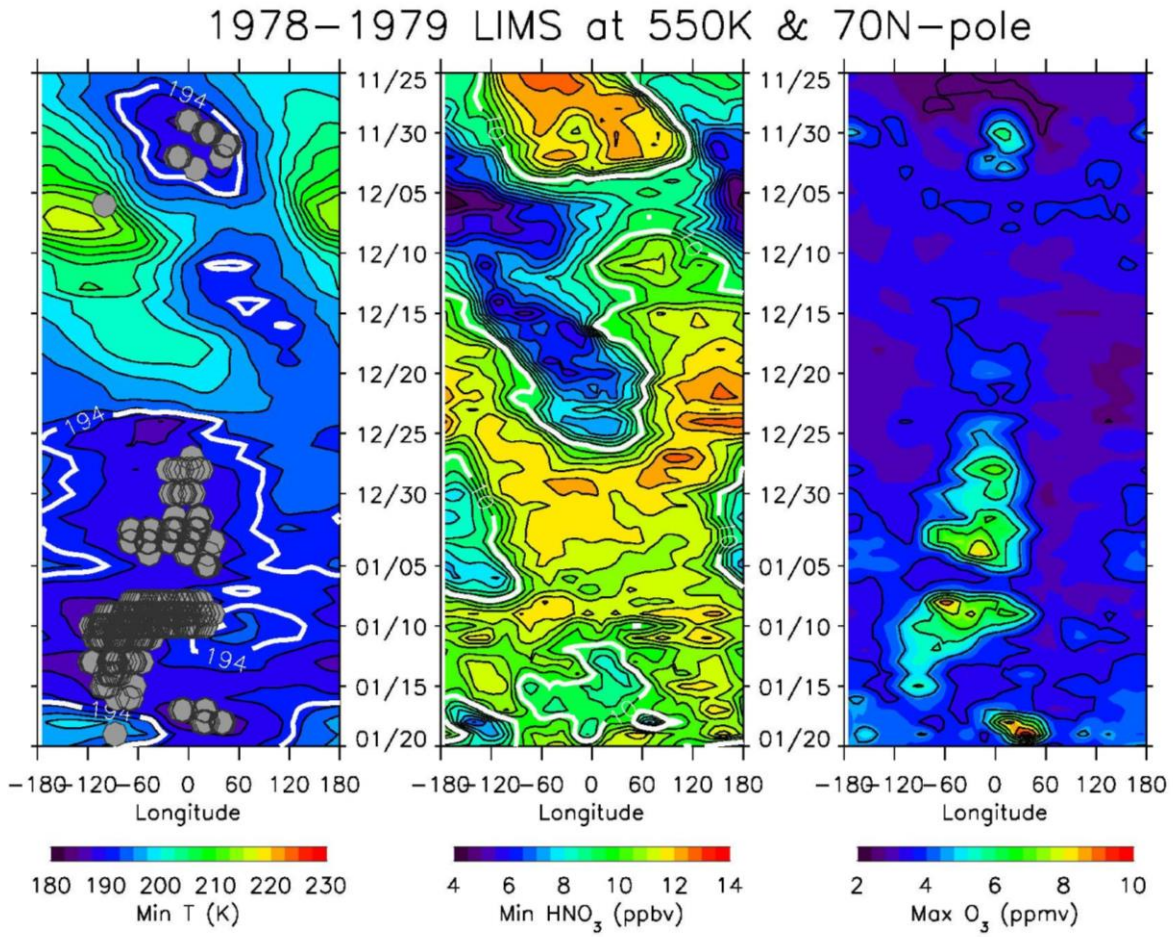

Figure 11— As in Fig. 10, but for the latitude domain of 70˚N to the Pole and from 25 November through 20 January; (left) fields of daily minimum temperature, (middle) daily minimum HNO_3, and (right) daily maximum ozone.

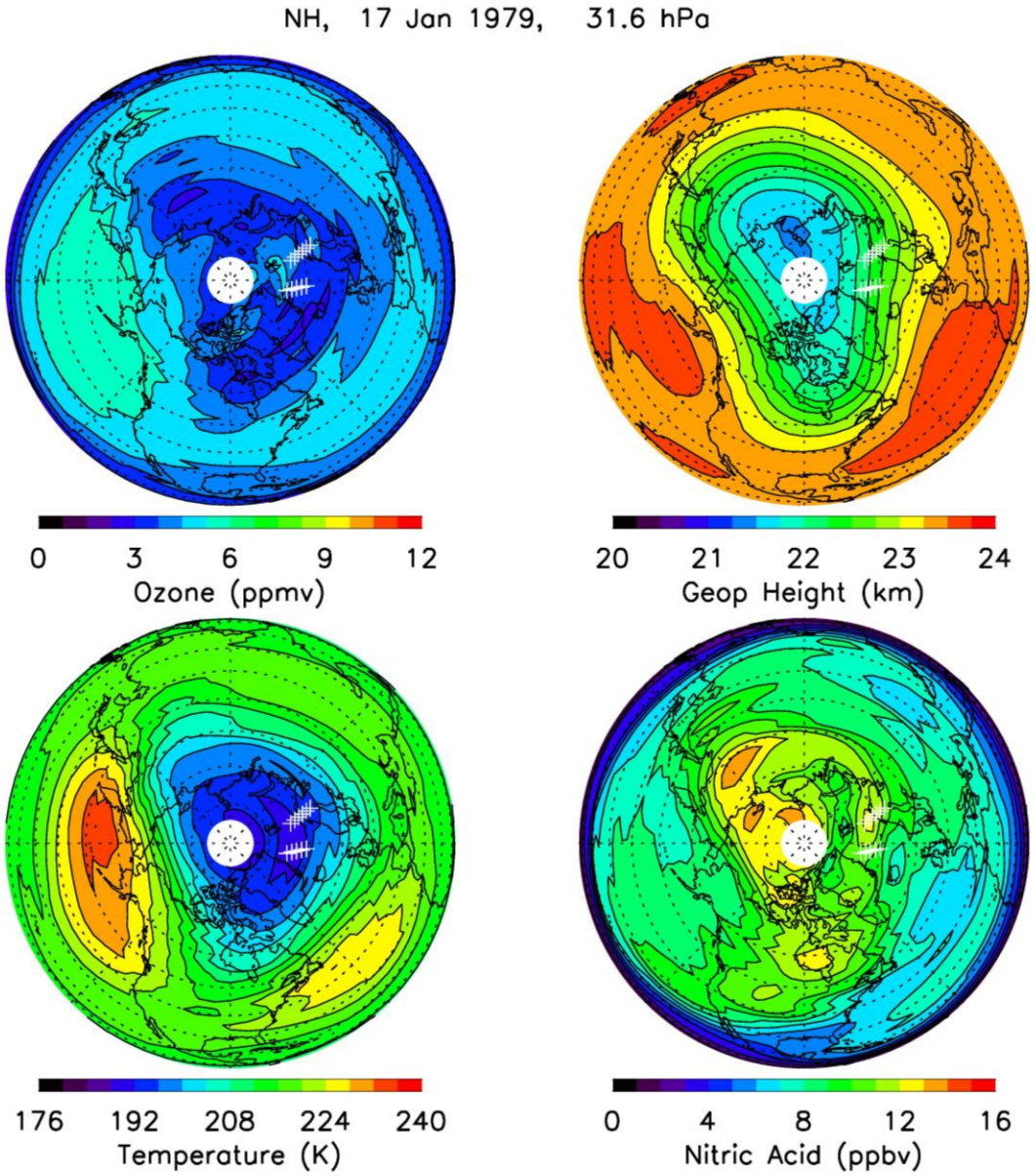

1159

1160 Figure 12—As in Fig. 2, but for 17 January.

1161

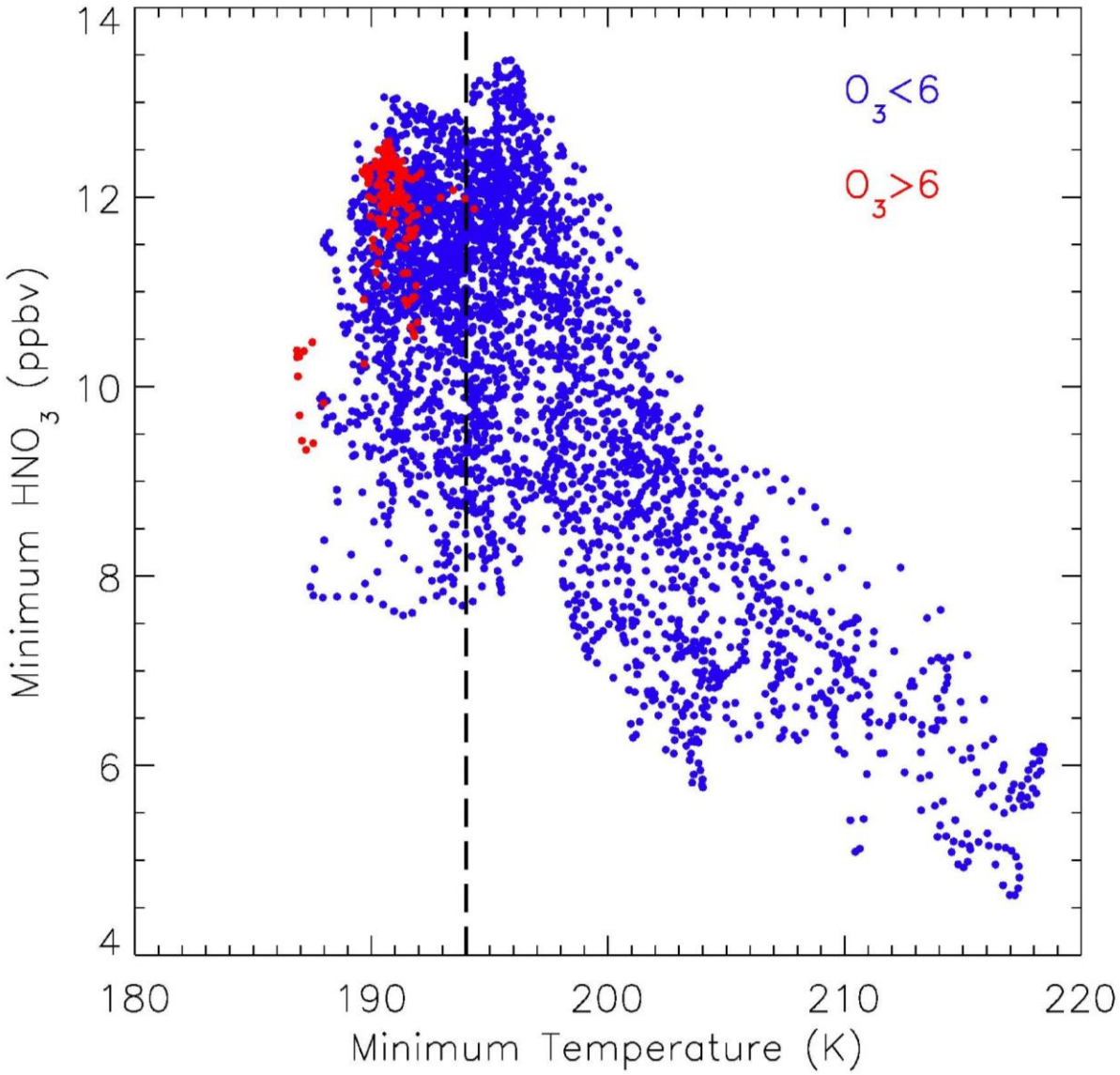

Figure 13— Scatterplot of minimum values of HNO_3 versus minimum values of temperature for the domain of 70˚N to the Pole at 550 K (from Figure 11); the vertical dashed line denotes 194 K. The corresponding maximum values of ozone are shown as red (> 6 ppmv) versus blue (<6 ppmv).

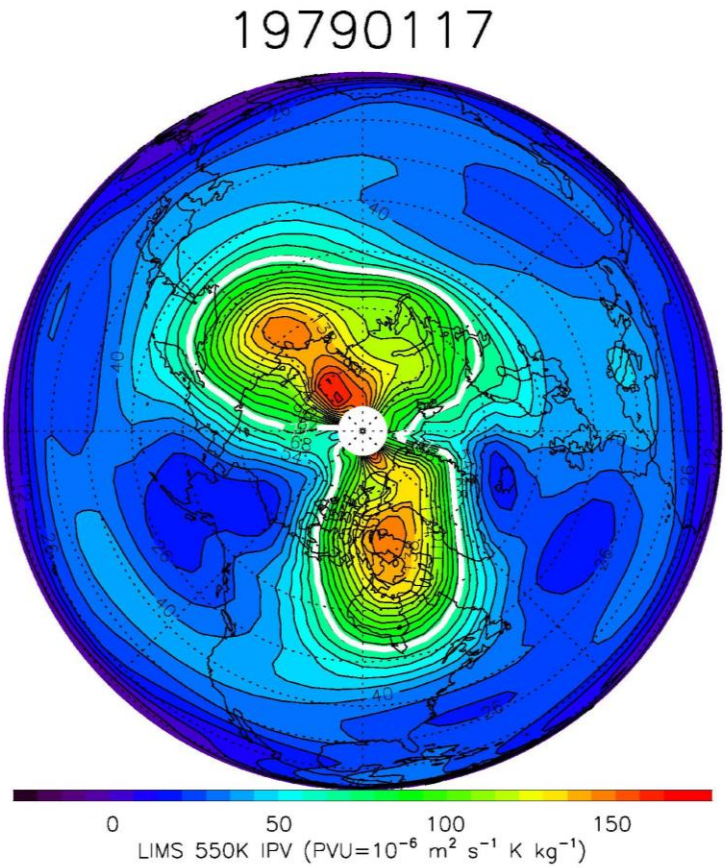

Figure 14—Isentropic potential vorticity (PV) at 550 K for 17 January 1979. Units of PV are in terms of (10^{-6} m^2 s^{-1} K kg^{-1}), and contour interval (CI) is 7 units. The thick white contour denotes the polar vortex edge as defined using Nash et al. (1996).

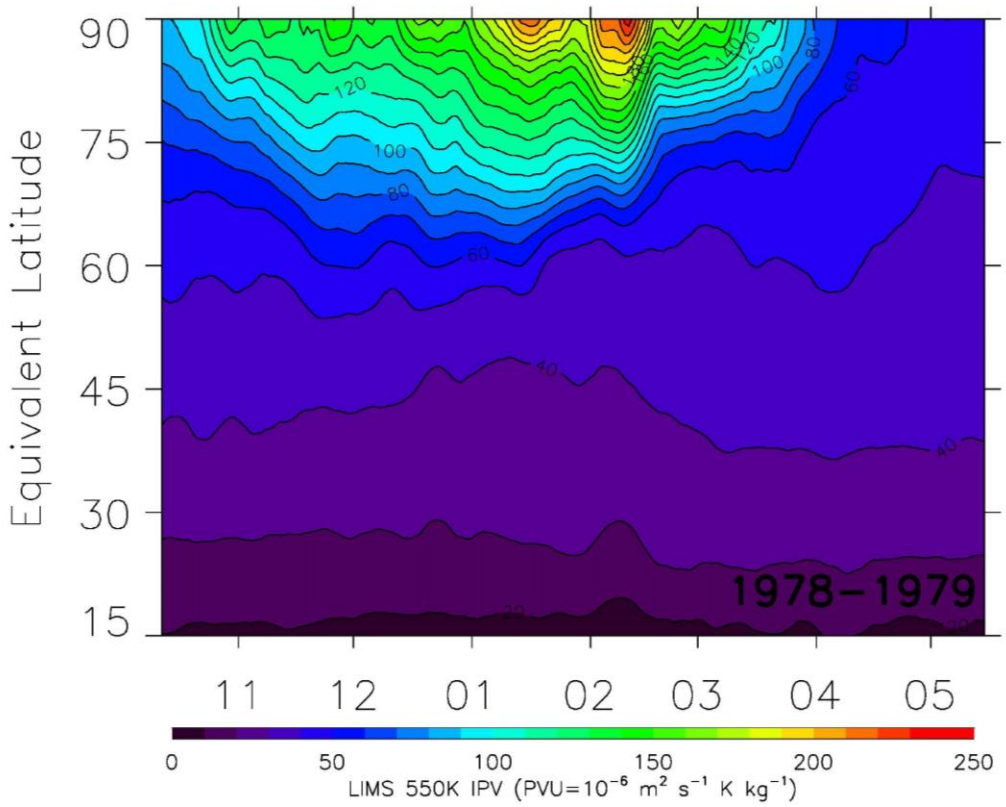

1173

1174 Figure 15—Time series of LIMS isentropic PV versus equivalent latitude at 550 K and with
1175 smoothing over 7 days. PV contour interval (CI) is 10 units.

1176

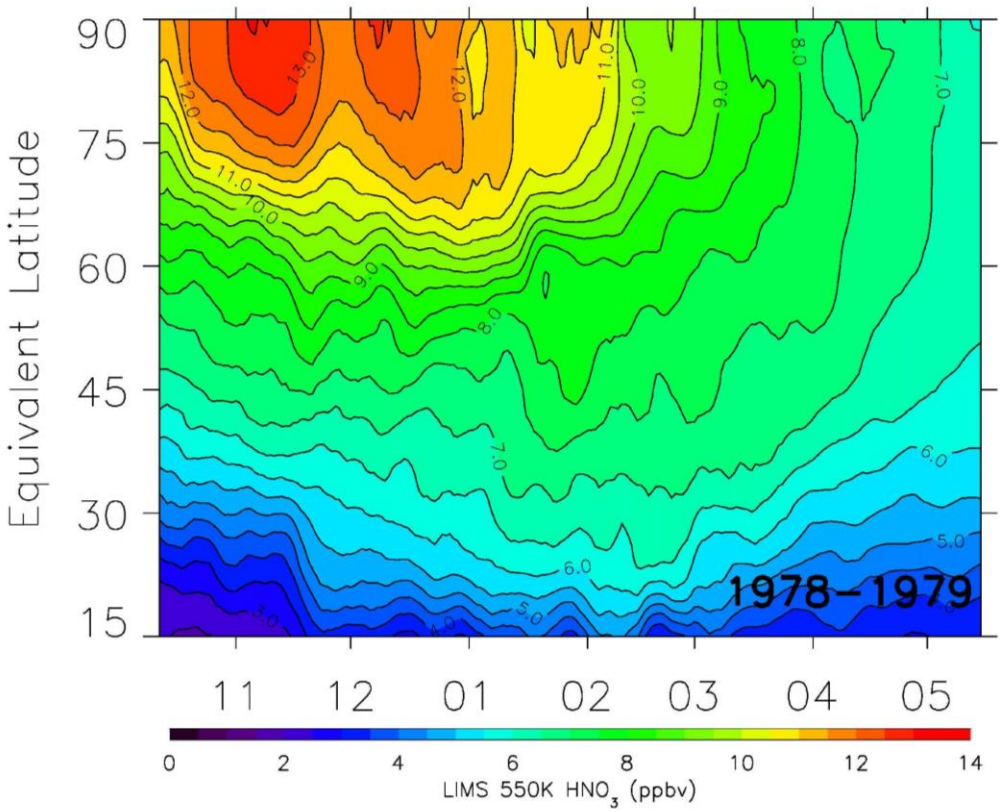

1177

1178 Figure 16—As in Fig. 15, but for HNO_3 (CI is 0.5 ppbv).

1179

1180

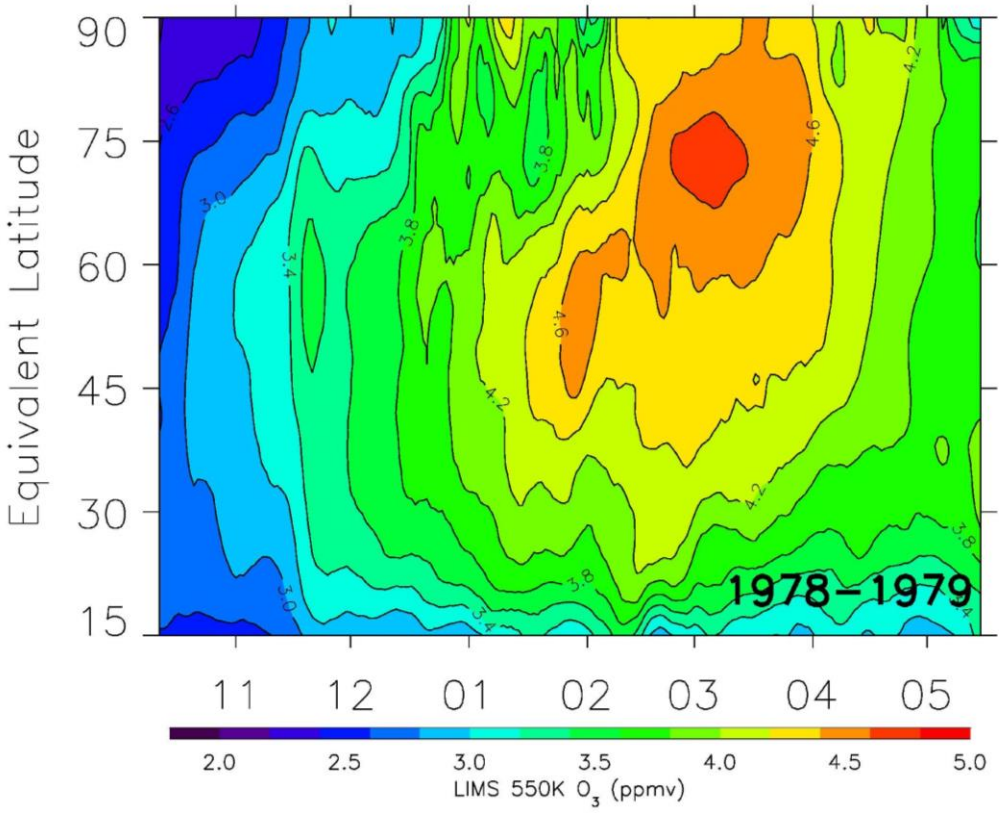

1181

1182 Figure 17—As in Fig. 15, but for ozone (CI is 0.2 ppmv).

1183

1184

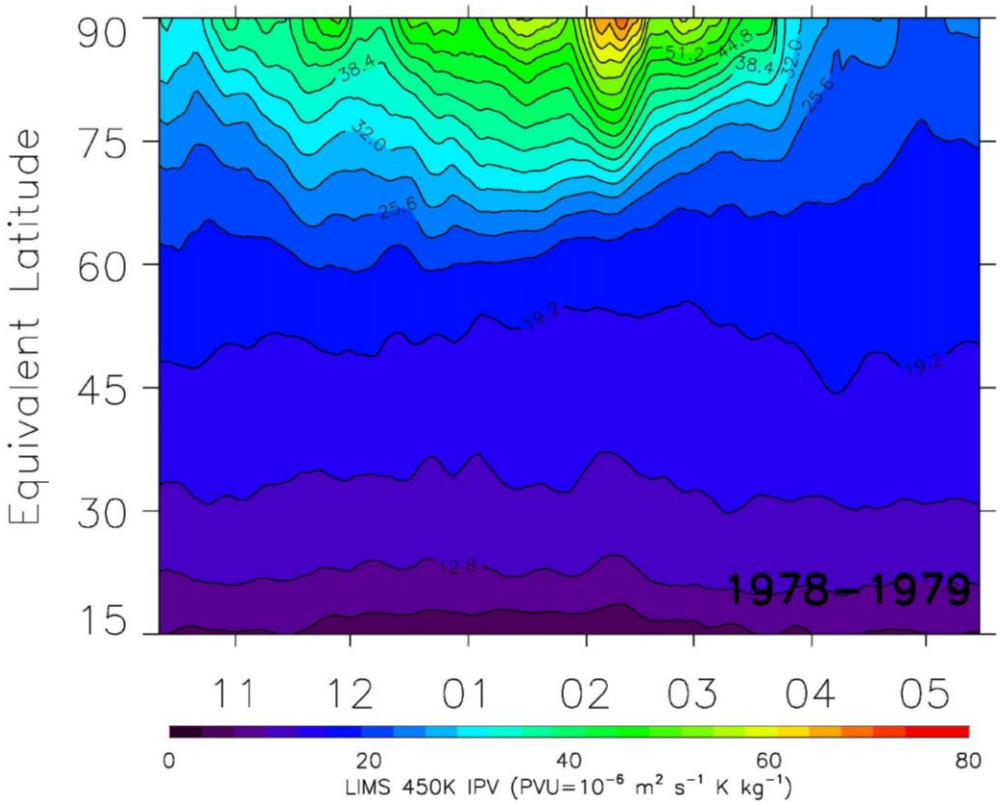

1185

1186 Figure 18—As in Fig. 15, but for PV versus equivalent latitude at 450 K (CI is 3.2 units).

1187

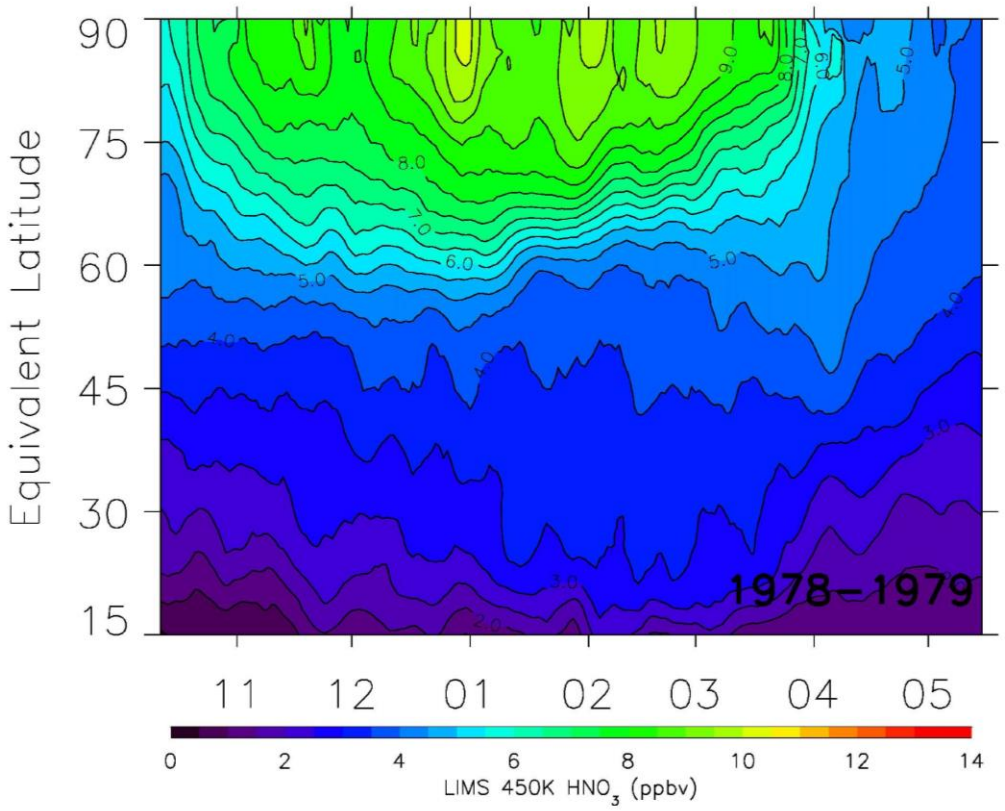

Figure 19—As in Fig. 16, but for HNO_3 at 450 K (CI is 0.5 ppbv).

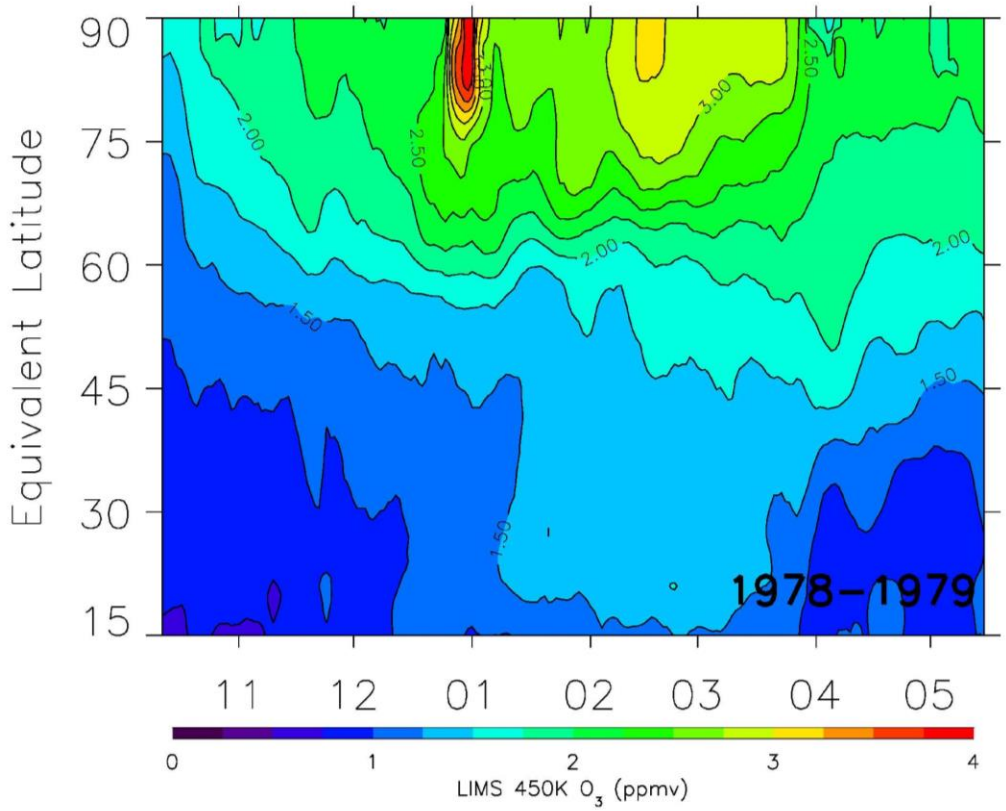

Figure 20—As in Fig. 17, but for ozone at 450 K (CI is 0.25 ppmv).